Correlation Function of Surface Systems with Dipole-dipole Interaction

Kiminori Kakitani

Correlation Function of Surface Systems with Dipole-dipole Interaction

Kiminori Kakitani

January 31, 1991

Abstract

The dipole-dipole interaction often plays important roles on the surface systems. The correlation function on the surface systems, where the dipole-dipole interaction extending to longer distance are assumed to be dominant, is theoretically investigated for the two examples, namely the alkali adsorbates on metal surface and the Si(100) reconstructed surface.

In the adsorbate system with repulsive dipole-dipole interaction, a set of approximate integral equations, which proposed on the basis of the high temperature expansion series at very low coverages in the disorder states, for two adsorbate correlation function is solved numerically. The correlation function obtained as a function of temperature and coverage is discussed with the experimental results of LEED and EELS.

Analysis on the phase transition of the Si(100) clean-surface reconstruction is made, in particular, on the two spin correlation function by computer simulation with emphasis on the short range order. The asymmetric dimer is described by a Ising spin and interactions short ranged as well as the dipole-dipole interaction are assumed between them. The anisotropy in the short range order above the transition point, which is observed experimentally, is examined in detail in the above mentioned model.

Acknowledgments

I would like to express my sincere gratitude to Professor Akio Yoshimori for introducing me to the surface physics and these problem of the thesis, encouragement and critical reading for the manuscript as well as stimulating discussions. I am also grateful to Professor Kikuo Cho, Dr. Kenji Makoshi, Dr. Yasushi Ohfuti and other members of Yoshimori resarch group for enlightening discussions, helpfull advices and valuable suggestions. This work was supported by a Grant in Aid for Scientific Research on Priority Areas of the Ministry of Education, Science and Culture of Japan. Numerical calculations were done on the SX-2 system at the Computer Center, Osaka University.

Contents

List of Tables

List of Figures

Chapter 1

Introduction

The statistical mechanics on surfaces is important for the investigation of the surface structure at finite temperatures, the surface reconstruction, the structure of the adsorbates on the surface, the phase transition on the surface and all phenomena which occur on the surface at the finite temperatures. The ground state structures can be pretty well discussed theoretically, for example, by *ab initio* total energy calculations of the electronic structure[1][2] and also by the rigorous method for possible arrangements of the surface atom or some adsorbates under some given interactions[3][4].

Of course many rigorous and approximate methods of statistical mechanics for two dimensional systems can be applied to surface properties. However, more development in methods is necessary to investigate surface properties of complex systems at finite temperatures. There are cases that the electric dipole-dipole interaction may play important roles in the surface system. Here the surface system means clean surfaces and adsorbate surfaces.

In this thesis, we deal with not only energy or specific heat, but also in very details with correlation function and short ranged ordered states.

1.1 Dipole-dipole interaction on surface systems

The dipole-dipole interaction can be important for surface properties. In the *bulk* of metals, the interaction for charged particle is screened, that is, Coulomb interaction which is long ranged become the short ranged screened Coulomb interaction.

On the metal surface, however, the Coulomb interaction is not always perfectly screened and there is some polarization because of the charged particles on the surface which is formed by the charge of the particle and its image charge. Whether the dipole on the surface is screened or not may be very sensitive to the position of the dipole. When the dipole is not screened, the dipole-dipole interaction can play a very important role on the surface. Of course the dipole-dipole interaction is convergent in a two dimensional system but it has no characteristic length and affects to longer distances. So the dipole-dipole interaction is never described by the interaction of a small number of near neighbors .

The statistical mechanics of such a system which has dipole-dipole interaction, have not yet been enough and satisfactory as far as we know, though some investigations have been made[5]. In this thesis, we try to discuss the statistical mechanics of such a system with focusing our attention on the correlation function and short ranged order.

1.2 Alkali metal atom adsorption

Alkali atoms on the metal surface, for example Na, K or Cs on Ni, Cu and so on, have been traditionally believed to be ionized at low coverages[6][7][8][9]. The alkali ions form electric dipoles with their image charges and separate each other by repulsive

force between dipoles. This model shows the linear dependence for the coverage of the work function at the low coverages. Recently, a different proposal for this system is given by Ishida et al.[2]. According to their *ab initio* calculation, alkali atoms are claimed not to be ionized, and the electric dipole for each adsorbate is given by a different origin. They believe that the dipole field is so weak and screened on the metal surface at the higher coverages where their calculation made.

The diffuse ring pattern is observed by low energy electron diffraction(LEED) for these alkali adsorbed systems[10]. The diameter of the ring pattern increases with coverages. This is in agreement with the model that adsorbates separate each other by certain strong repulsive force.

In this thesis, we do not address whether alkali atoms are ionized or not but discuss the statistical mechanics where the dipole-dipole repulsive interaction is assumed to be a dominant interaction between alkali adsorbates. When the coverage is low, the adsorbates are rather well separated by the strong repulsive dipole-dipole interaction and they do not come to neighboring sites. With this reason, we assume that only the dipole-dipole interaction is dominant and the near neighbor interaction, for example electronic origin, can be neglected.

1.3 Asymmetric dimer on Si(100)

It is well known that Si(100) clean surface has a 2×1 reconstruction at room temperature. This reconstruction is explained by the *dimer* model. Each two Si atoms on the top layer of the surface makes a dimer as shown in Figure 1.1. The total energy calculation of the tight binding scheme shows that the asymmetric dimer is

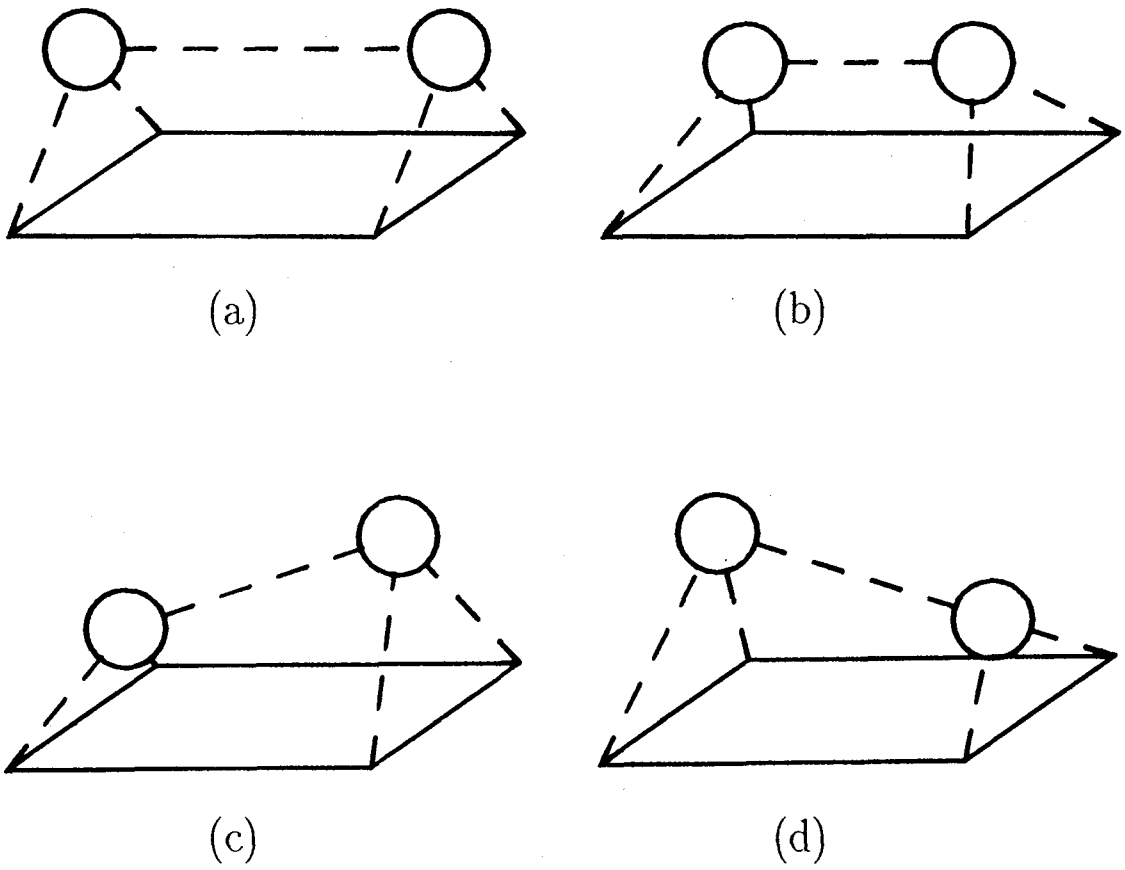

The circles mean Si atoms on the top layer of Si(100) surface. The Si atoms of the second layer are on the corner of the rectangle. (a) is the ideal surface and (b) shows the symmetric dimer. (c) and (d) are two sorts of the asymmetric dimer, respectively.

Figure 1.1: Dimer on Si(100) surface

more stable than the symmetric dimer[13].

In the topography of the Scanning Tunneling Microscopy(STM), it seems that symmetric dimers are arranged on the plane surface[14]. The asymmetric dimer is observed only around some defects. The core level shift of the Si atom observed by X-ray photoemition spectroscopy(XPS) does not show the difference between two Si atoms which make the dimer[16]. Although the symmetric dimer model is not denied absolutely, the idea that the asymmetric dimer flips its direction faster than STM scans each asymmetic dimer can explain the topography of STM. According to Yamazaki and Cho [15], the problem of the core level shift does not contradict with asymmetric dimer when one takes into account a final state interaction effect. The result of the *ab initio* calculation with density functional scheme by Zhu et al.[1] shows that the ground state is the c(4×2) structure based on the asymmetric dimer model. In the asymmetic dimer model, two Si atoms in each dimer is not equivalent. Each dimer has a polarization caused by asymmetry of the bonding charge. The dipole-dipole interaction may play an important role in this system.

In this thesis, we assume the asymmetric dimer model with a dipole moment for the Si(100) surface and discuss the short ranged order with strong anisotropy caused by dipole-dipole interaction between asymmetric dimers.

Chapter 2

Alkali metal atom adsorption on metal surface

2.1 Experimental results

The adsorption of the alkali metal atoms on transition metal surfaces is important because of the work function lowering[17][18] and the adsorption induced reconstruction[19] and also known as the *poison* of the catalysis, so many kinds of experiments have been performed. They can give some important information for the study of the surface structure at finite temperatures and the dipole on the surface.

2.1.1 Structural analysis

The diffraction patterns of alkali adsorption metal surface system observed by LEED give some structural information[19]. The increase of back ground intensity is observed at very low coverages. It is supposed to be due to the random arrangement of the alkali metal atoms on the metal surface. The diffuse ring pattern appears as the coverage increases. For example, this ring pattern is observed at θ ~0.12–0.13 for the system of K on Ni(100) surface. The diameter of this ring pattern is said to be proportional to square root of the coverage[19]. This ring pattern may be due

to short range correlation caused by the existence of the strong and longer ranged repulsive interaction.

2.1.2 Work function

The typical coverage dependence of the work function of this system is shown in Figure 2.1. The work function is proportional to the coverage at low coverage region and have the minimum at a certain coverage. This variation of the work function is corresponding to the variation of the dipole layer formed by alkali metal adsorbates. At very low coverages, each adsorbate forms a dipole moment and the work function depends on only the density of the dipole moment on the surface. But the magnitude of the dipole moment varies itself at higher coverage where the minimum is observed. This dipole moment may be formed by the alkali metal ion on the metal surface and its screening (image) charge. The bonding of alkali metal atoms is not negligible at high coverages. The recent *ab initio* calculation claims that the 'Alkali ion' picture is not correct[2].

2.1.3 Spectroscopic analysis

Information about electronic structure of this system is obtained by electron energy loss spectroscopy(EELS). The broad peak is observed by the EEL spectra of this system at ~3–5eV. This peak may be understood as the excitation that an electron is excited from Fermi surface to the unoccupied level localized on the adsorbate. This peak energy also depends on the coverage and is said to be proportional to $\theta^{3/2}$. This coverage dependence may be related to the mean potential which an adsorbate receives from another adsorbate.

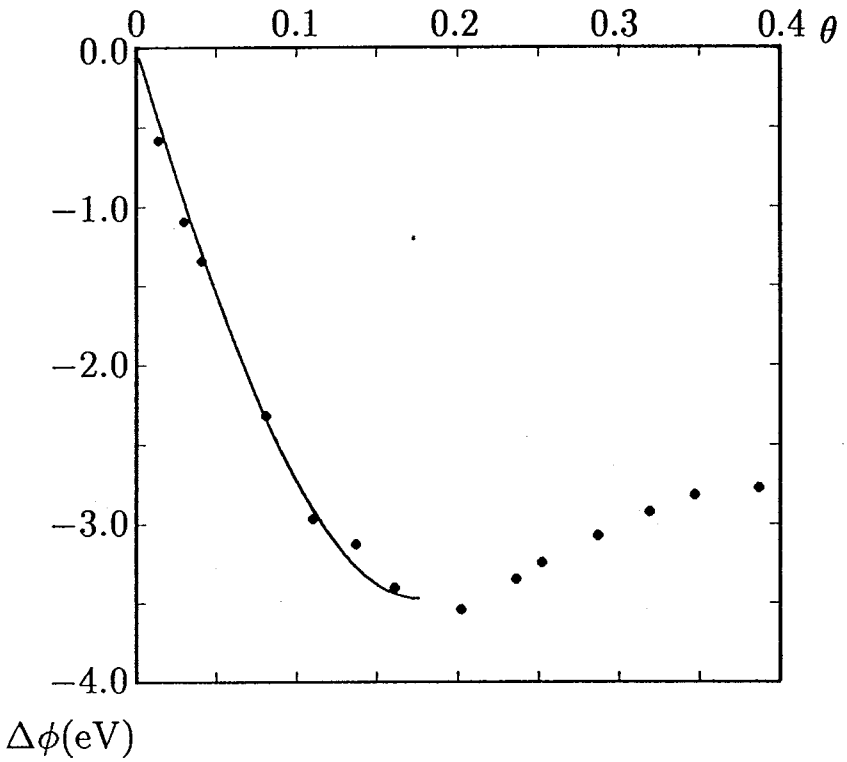

Figure 2.1: The coverage dependence of the work function change

Filled circles are experimental values of K on Ni(100) obtained by Anderson and Jostel[18] and the solid curve is their fitting with the fictitious adsorbate lattice assumption.

2.2 Theoretical Study

2.2.1 Lattice gas model

Almost every adsorbate on the crystalline surface has its own energetically favorable sites for adsorption. So the lattice gas model is suitable for many adsorption systems. In this analysis, the adsorbate sites are assumed to form a two-dimensional Bravais lattice on the substrate surface. The occupation number of adsorbate at the i-th site is denoted by n_i. The Hamiltonian of the lattice gas system with dipole-dipole interaction is given by

$$\mathcal{H} = \frac{1}{2}\sum_{i,j} J_{ij} n_i n_j \tag{2.1}$$

and

$$J_{ij} = \frac{\mu_0^2}{|r_i - r_j|^3} \tag{2.2}$$

where μ_0 is the magnitude of the dipole moment of the adsorbate and r_i is the position vector of the i-th site of the adsorbate. The grand partition function, Ξ, of the system is given by

$$\begin{aligned} \Xi &= \mathrm{tr}\exp\{-\beta(\mathcal{H} - \mu\mathcal{N})\}, \\ \mathcal{N} &= \sum_i n_i, \end{aligned} \tag{2.3}$$

where μ is the chemical potential. The coverage, θ, is controlled by the chemical potential and determined by

$$\theta = \frac{1}{M}\langle\mathcal{N}\rangle = \Xi^{-1}\mathrm{tr}\frac{1}{M}\sum_i n_i e^{-\beta(\mathcal{H}-\mu\mathcal{N})}, \tag{2.4}$$

where M is the total number of the sites. The correlation function of two adsorbates is defined by

$$\langle n_i n_j \rangle = \Xi^{-1} \mathrm{tr} n_i n_j e^{-\beta(\mathcal{H}-\mu\mathcal{N})}. \tag{2.5}$$

2.2.2 Ordered structure on ground state

The ordered structure on the ground state for the lattice gas system which has the repulsive interaction presented by the power of the distance between two particles on the Bravais lattice, is already studied by Pokrovsky and Uimin[5], when the coverage is given by $1/p$, where p is a positive integer.

In this simplest case, according to Pokrovsky and Uimin, particles form the quasi-triangular lattice which is commensurate to the substrate in the ground state as intuition tells us for the repulsive force, and the ground state energy, E_0, of the lattice gas system particularly with the dipole-dipole interaction is obtained as follows.

When the fundamental lattice vectors of the lattice of possible adsorbed sites, which is assumed to be the Bravais lattice, are denoted by $\boldsymbol{a}_0$ and $\boldsymbol{b}_0$, the fundamental lattice vectors of the lattice formed by adsorbates, $\boldsymbol{a}$, $\boldsymbol{b}$ are written by

$$\begin{aligned} \boldsymbol{a} &= k_0 \boldsymbol{a}_0 + \ell_0 \boldsymbol{b}_0, \\ \boldsymbol{b} &= m_0 \boldsymbol{a}_0 + n_0 \boldsymbol{b}_0, \end{aligned}$$

where k_0, ℓ_0, m_0 and n_0 are integer. The coverage is given by

$$\theta = |k_0 n_0 - m_0 \ell_0|^{-1}.$$

Table 2.1: Ordered structures for the square lattice

p	θ	$\boldsymbol{a}$ (k_0, ℓ_0)	$\boldsymbol{b}$ (m_0, n_0)	ζ	$\cos\phi$	$f(\zeta,\phi)$
16	0.0625	(4, 0)	(1, 4)	1.109	0.526	4.428
17	0.0588	(7, 2)	(2, 3)	0.522	0.870	4.430
18	0.0556	(6, 0)	(2, 3)	0.687	0.728	4.482
19	0.0526	(7, 1)	(2, 3)	0.558	0.809	4.451
20	0.0500	(5, 0)	(1, 4)	0.887	0.526	4.432

This table shows the informations of the ordered state which has the lowest energy for given p. These ordered state was obtsined by Pokrovsky and Uimin[5].

The total energy is represented by

$$E_0 = N\mu_0^2\theta^{3/2} f(\xi,\phi), \tag{2.6}$$

where N is total number of adsorbates, ξ is the ratio of lengths of the lattice vector, $\frac{|\boldsymbol{a}|}{|\boldsymbol{b}|}$ and ϕ is the angle between the lattice vector $\boldsymbol{a}$ and $\boldsymbol{b}$. $f(\zeta,\phi)$ is given by

$$f(\zeta,\phi) = (\sin\phi)^{-3/2}\left\{\sum_{k=1}^{\infty}\sum_{\ell=1}^{\infty}\left[(\xi k^2 + \frac{1}{\xi}\ell^2 + 2k\ell\cos\phi)^{-3/2}\right.\right.$$

$$\left.\left. +(\xi k^2 + \frac{1}{\xi}\ell^2 - 2k\ell\cos\phi)^{-3/2}\right] + \zeta(3)(\xi^{-3/2} + \xi^{3/2})\right\},$$

where $\zeta(x)$ is the Riemann zeta-function and $\zeta(3) = 1.202056\cdots$.

For the quasi-triangular lattice of the ground state, one can find from the expression (2.6) that $f(\zeta,\phi)$ is almost constant as in Table 2.1. The potential energy value at a particle from the other particles is obtained as in the same form. So the dipole field of an adsorbate is almost proportional to $\theta^{3/2}$ on the ground states.

2.2.3 High temperature expansion

The information on the short-range order can be drawn from two particle correlation function. The problem to obtain the correlation function of the lattice gas system is to obtain an effective interaction which acts upon each particle on the lattice from the others. The effective interaction between the adsorbate on the i-site and on the j-site, $\mathcal{J}_{ij}$, is defined by the correlation function denoted by $\langle n_i n_j \rangle = \theta^2 \exp\{-\mathcal{J}_{ij}\}$. This effective interaction can be obtained by high temperature expansion method when the coverage is very low[20]. In the following, throughout in this chapter, we assume that there is no long range order in the system.

The high temperature expansion results for the quantities, Ξ, θ and $\langle n_i n_j \rangle$ are as follows (they are listed up in Appendix up to 4th order).

$$\Xi = 1 - \beta \sum_{12} J_{12} c^2 + \cdots. \tag{2.7}$$

$$\theta = c - \left(\frac{\beta}{2}\right)\left[2\sum_{1} J_{i1} c^2 + \sum_{1,2\neq i} J_{12} c^3 - \sum_{1,2} J_{12} c^3\right] + \cdots, \tag{2.8}$$

$$\begin{aligned}\langle n_i n_j \rangle = {} & c^2 - \left(\frac{\beta}{2}\right)\left[2\sum_{1\neq j} J_{i1} c^3 + 2\sum_{1\neq i} J_{1j} c^3 + 2 J_{ij} c^2\right. \\ & \left. + \sum_{1,2\neq i,j} J_{12} c^4 - \sum_{12} J_{12} c^4\right] + \cdots,\end{aligned} \tag{2.9}$$

where 1 and 2 abbreviate running indices, ℓ_1 and ℓ_2, respectively, and c is the coverage of the non-interacting system, defined by

$$c = \frac{1}{1 + e^{-\beta\mu}}. \tag{2.10}$$

Here for example in (2.9), the third term in the square bracket cancels almost the second term exclusive of the case of $\ell_1(\ell_2) = i$. Similar cancellations occur in

each expansion, which correspond to the linked cluster expansion theorem. So Ξ, θ and $\langle n_i n_j \rangle$ are obtained as follows.

$$\begin{aligned}
\Xi &= \exp\left\{-\beta \sum_{12} J_{ij} c^2 + \left(\frac{\beta}{2}\right)\left[2\sum_{123} J_{12}J_{23}c^3(1-c) + \sum_{12} J_{12}^2 c^2(1-c)^2\right] - \cdots\right\}, \\
\theta &= c - \left(\frac{\beta}{2}\right) 2\sum_{1} J_{i1} c^2(1-c) + \cdots, \\
\langle n_i n_j \rangle &= c^2 - \left(\frac{\beta}{2}\right)\left[2\sum_{1} J_{i1}c^3(1-c) + 2\sum_{1} J_{1j}c^3(1-c) + 2J_{ij}c^2(1-c)^2\right] + \cdots.
\end{aligned} \tag{2.11}$$

2.2.4 Diagram analysis

The high temperature expansion in the previous section can be described by diagrams[20]. For example, the expansion of the partition function is represented by

$\Xi = 1 +$ 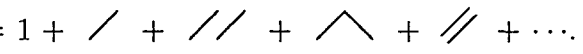 $+ \cdots.$

These diagramatical expressions correspond to the analytical expression by following rules,

1. Each line corresponds to the interaction $-\beta J_{ij}$.

2. *End* points and *joint* points of lines represent the site indices of J_{ij}, which are summed up over all lattice points.

3. The *end* points and *joint* points of lines are corresponding to certain functions of c. For example a lone *end* point, that is, a simple line end, corresponds to c and a *joint* point of two lines and three lines correspond to $c(1-c)$ and

$c(1-c)(1-2c)$, respectively. Generally $F_n(c)$ corresponding to the *joint* points of n lines is obtained as

$$F_n(c) = c(1-c)\frac{\partial}{\partial c}F_{n-1}(c) \tag{2.12}$$

$$F_1(c) = c \tag{2.13}$$

These relations are proven by Green function method (see 2.4.1).

4. The coefficient of each graph, which is supposed to be included in the graph of the graphical representation, is the number of all possible equivalent arrangement which are obtained by exchanging the running indices.

The expansion of θ is represented by

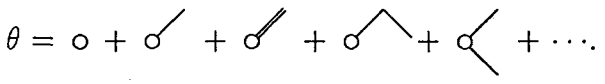

where open circles denote the fixed i site which is not summed up. The correlation function, $\langle n_i n_j \rangle$ is expanded as

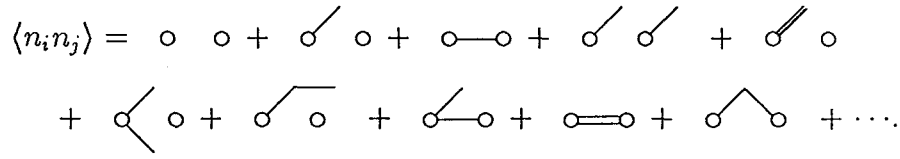

where open circles denote i and j sites. Particularly the *end* points with open circle are corresponding to $c(1-c)$.

When θ is so small as

$$c = \frac{1}{1+\exp(-\beta\mu)} \approx \exp(\beta\mu), \tag{2.14}$$

the interaction denoted by the line with free end may be renormalized in the coverage, θ, for example, as follows.

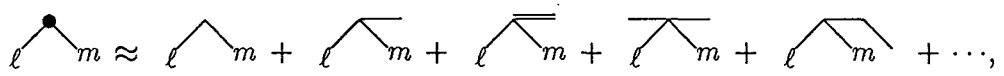

where *end* points named ℓ and m are fixed or connected to other graphs, and the other *end* points and *joint* points presents indices which are summed up independently. Solid circles corresponds to renormalized coverage, θ. The correlation function can be rewritten as

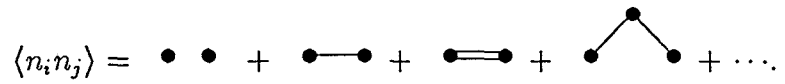

These graphs are corresponding to the following expansion,

$$\langle n_i n_j \rangle = \theta^2 - \beta J_{ij}\theta^2 + \frac{\beta^2}{2!}{J_{ij}}^2\theta^2 + 2!\frac{\beta^2}{2!}\sum_k J_{ik}J_{kj}\theta^3. \tag{2.15}$$

These renormalized diagrams for correlation function at low coverages corresponds to the analytical expressions by following rules.

1. Each solid fine line corresponds to the $-\beta J_{ij}$.

2. Two *end* points and *joint* points of lines give the site indices of J_{ij}.

3. Two *end* points have also site indices of the correlation function $\langle n_i n_j \rangle$.

4. The site indices given by *joint* points are summed up over all lattice points.

5. All *end* points and *joint* points correspond to the renormalized coverage, θ.

6. The coefficient of each graph, included in the graph of the graphical representation, is the number of all possible equivalent arrangement which are obtained by exchanging the running indices.

There are three sorts of diagram in this expansion. The first two are *reducible*, and are classified into the *open* graph and the *closed* graph. The *closed* graphs are decomposed into more than two graphs by cutting the graph into parts at both *end* point. Followings are typical *closed* graphs,

The *open* graphs are decomposed into more than two parts by cutting the graph into parts at a *joint* point. Followings are typical *open* graphs,

The last is the remaining ones, that is, the *irreducible* graphs described in the cluster expansion theory as follows,

One can find that all *open* graphs are constructed by products of Fourier components of the *irreducible* graphs and the *closed* graphs. We define that the effective interaction, $\mathcal{J}_{ij}$, is the summation of all *irreducible* graphs and *open* graphs, so that

summation of all over the graphs actually having the correct coefficients for the exponential expansion, which denotes the correlation function, can be obtained as

$$\langle n_i n_j \rangle = \theta^2 \exp\{-\mathcal{J}_{ij}\}. \tag{2.16}$$

The effective interaction is rewritten by the graphs as follows,

where the wavy line is the effective interaction.

The summation of all the *close* graphs and *irreducible* graphs is defined as follows,

where we express this summation by a line with a box like the graph on the left hand side.

All the *closed* graphs are constructed by products of summations in real space and each part of their products is represented by a *irreducible* graph or a *open* graph. The effective interaction can be described as the following graphical sum,

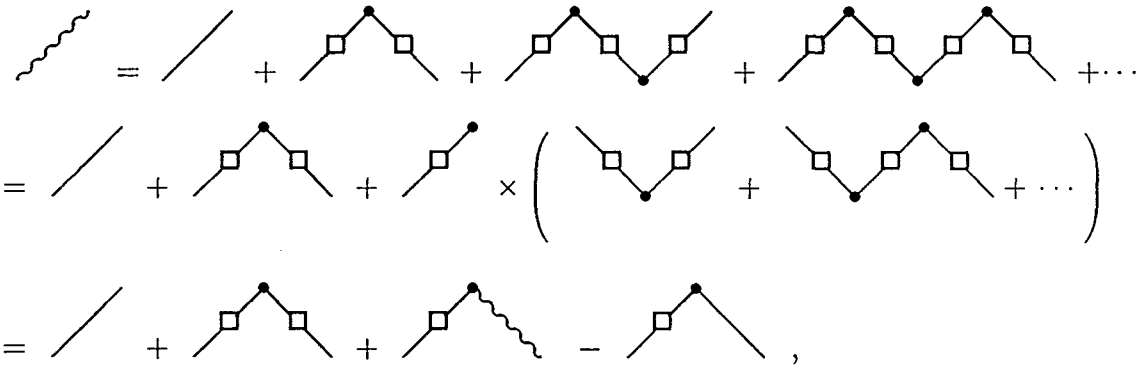

where the solid broad line does not represent the $-\beta J_{ij}$ but the summation of all *irreducible* graphs. This series of graphs are valid inclusive their coefficients.

The summation of all sorts of graphs gives the correlation function, one can obtain following relation.

$\langle n_i n_j \rangle =$ 

So the relation between graphs is obtained as follows,

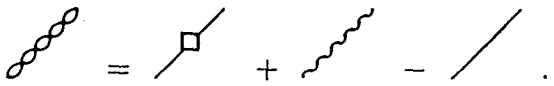

where a *chain* represents a function $\mathcal{L}_{ij}$ defined by

$$\mathcal{L}_{ij} = \exp(-\mathcal{J}_{ij}) - 1. \tag{2.17}$$

The closed relation between the graphs of $\mathcal{J}_{ij}$ and $\mathcal{L}_{ij}$ can be obtained by use of previous relations of graphs as follows,

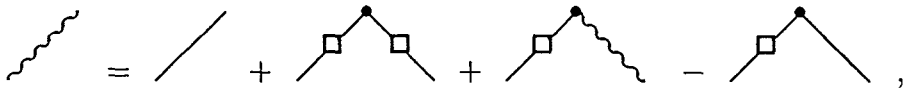

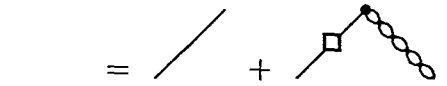

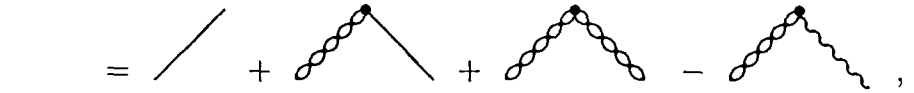

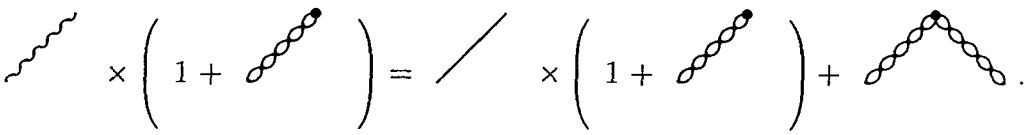

These diagramatical expressions are corresponding to the following equation,

$$-\mathcal{J}(k) = \Sigma^{(ir)}(k) + \frac{\theta\mathcal{L}(k)^2}{1+\theta\mathcal{L}(k)}, \tag{2.18}$$

where $\Sigma^{(ir)}$ is the Fourier component of the summation of all *irreducible* graphs. $\mathcal{J}(k)$ and $\mathcal{L}(k)$ are the Fourier component of $\mathcal{J}_{ij}$ and $\mathcal{L}_{ij}$, respectively. When we substitute only $-\beta J_{ij}$ for the summation of all *irreducible* graphs, we can get the same set of equations as our previous paper[21]. Here we get a set of self-consistent integral equations for the effective interaction and the correlation function as follows,

$$\begin{aligned} \mathcal{J}_{ij} &= \beta J_{ij} - \sum_{k} \frac{\theta\mathcal{L}(k)^2}{1+\theta\mathcal{L}(k)} e^{ik\cdot r_{ij}}, \\ \mathcal{L}(k) &= \sum_{r_{ij}} \left(\exp\{-\mathcal{J}_{ij}\} - 1\right) e^{-ik\cdot r_{ij}}. \end{aligned} \tag{2.19}$$

2.2.5 Numerical solution

It is not very easy to find the solution of the set of equations(2.19) even by numerical calculation. Since the dipole-dipole interaction extends to a longer distance, we have to make the system larger to have the summention convergent in the numerical calculation.

Since the set of equations(2.19) is valid for the state without long-range order, we may assume that there is a certain distance R_c and $\mathcal{J}_{ij} << 1$ for $|r_i - r_j| \geq R_c$. Then $e^{-\mathcal{J}_{ij}}$ can be replaced by $1 - \mathcal{J}_{ij}$ for $|r_i - r_j| \geq R_c$. Then the equation(2.19)

is rewritten as

$$\mathcal{L}(\boldsymbol{k}) = \sum_{|\boldsymbol{r}_i-\boldsymbol{r}_j|<R_c} \left[e^{-\mathcal{J}_{ij}} - 1 + \mathcal{J}_{ij}\right] e^{-i\boldsymbol{k}\cdot(\boldsymbol{r}_i-\boldsymbol{r}_j)} - \mathcal{J}(\boldsymbol{k}), \tag{2.20}$$

$$\mathcal{J}(\boldsymbol{k}) = \sum \mathcal{J}_{ij} e^{i\boldsymbol{k}\cdot(\boldsymbol{r}_i-\boldsymbol{r}_j)}. \tag{2.21}$$

Together with,

$$\mathcal{J}_{ij} = \beta J_{ij} - \sum_{\boldsymbol{k}} \frac{\mathcal{L}(\boldsymbol{k})^2\theta}{1+\mathcal{L}(\boldsymbol{k})\theta} e^{i\boldsymbol{k}\cdot(\boldsymbol{r}_i-\boldsymbol{r}_i)}, \tag{2.22}$$

(2.20) and (2.21) form a set of equations to determine $\langle n_i n_j \rangle$. The correlation functions at given temperatures and given coverages are calculated numerically by solving this set of equations.

Correlation function

The correlation function is calculated for several systems. The $\frac{\mu_0^2}{a_0^3}$ is the only parameter which determines properties of this model. For alkali adsorbate systems, a_0 is the lattice constant of the two dimensional lattice of the metal surface and the dipole moment μ_0 is determined from the slope of the θ-dependence of the work function at $\theta = 0$.

The values of $\frac{\mu_0^2}{a_0^3}$ in numerical calculation are so chosen that they correspond to Na on Ni(100), K on Ni(100) and K on Cu(100) of which the coverage dependent diffuse ring in LEED are observed. The β is the reciprocal of the temperature.

The values of β corresponding to room temperature(T=300K) and $\frac{\mu_0^2}{a_0^3}$ for the several systems are shown in Table 2.2 with $k_B = 1$ and $\frac{e^2}{a_B^3} = 1$ where k_B, e and a_B are Bolzmann constant, the charge of an electron and Bohr radius, respectively. Throughout this section, this unit system is used. $\langle n_i n_j \rangle$ and $F(\boldsymbol{k})$ at several tem-

Table 2.2: Dipole moments for alkali adsorption systems

	μ_0(a.u.)	d(Å)	$\frac{\mu_0^2}{a_0^3}$(eV)	$\beta_{T=300K}$
Na/Ni(100)	2.83	0.75	2.1	40.0
K/Ni(100)	4.26	1.13	4.8	90.0
K/(Cu(100)	6.60	1.73	10.5	200.0

d is the distance between the adsorbate and the metal surface and determined with the assumption that each alkali metal atom is ionized completely. $\beta_{T=300K}$ is the value of β corresponding to room temperture(T=300K).

peratures and $\theta = 0.03$ are shown in Figure 2.2a and Figure 2.2b, where $F(k)$ is the component of Fourier transform of $\langle n_i n_j \rangle$ and corresponding to the structure factor of diffuse LEED. It is defined as,

$$F(k) \equiv 1 - \theta + \theta \sum_{i \neq j} (e^{-\mathcal{J}_{ij}} - 1) e^{i\boldsymbol{k}\cdot(\boldsymbol{r}_i - \boldsymbol{r}_j)} \tag{2.23}$$

R_c is taken to be $40a_0$ or $60a_0$. Of course it is confirmed that $\mathcal{J}(r)$ is so small that $e^{-\mathcal{J}(r)} \sim 1 - \mathcal{J}(r)$ at $|r| \geq R_c$ for these numerical results.

Figure 2.2a shows that the adsorbate can not approach on the nearest site even at the high temperature. The peak is found at $r_{ij} = 6$ that is almost corresponding to the nearest neighbor distance of the ordered lattice formed by adsorbates on ground state for $\theta = 0.03$. The intensity of this peak increases as the temperature decreases. This short range order is more remarkable at lower temperatures and larger dipole moments. A stereogram of the Fourier components of the correlation function, $F(k)$, is sketched in Figure 2.3. $F(k)$ is corresponding to the structure factor of LEED as mentioned above. The clear ring shape is found at the temperature where the short

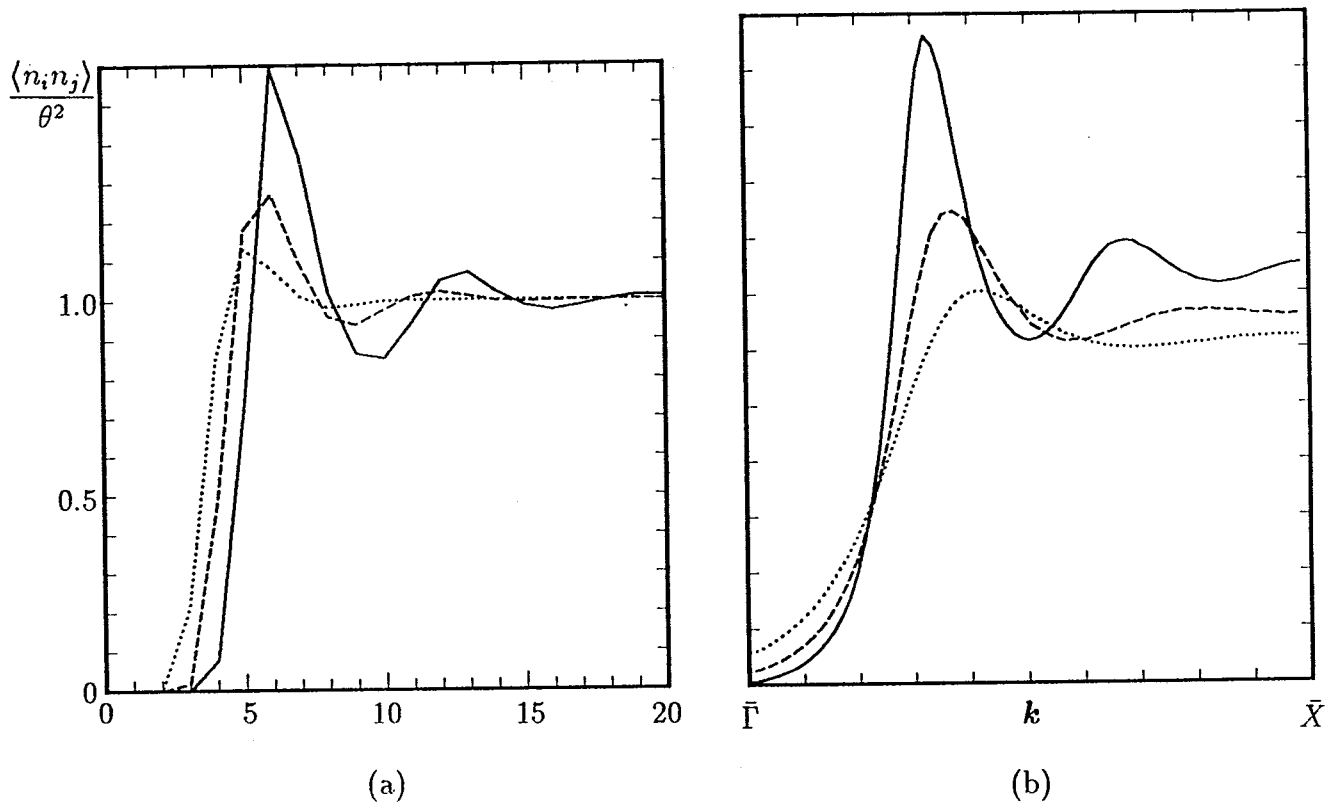

Figure 2.2: Calculated correlation function at $\theta = 0.03$

(a):The correlation function, $\langle n_i n_j \rangle$, along the $\langle 10 \rangle$ direction
(b):The structure factor along $\bar{\Gamma}$—$\bar{X}$ direction
The solid curve, the dashed curve and doted curve are the results and $\beta = 40$, $\beta = 90$ and $\beta = 200$, respectively. These are calculated at $\theta = 0.03$.

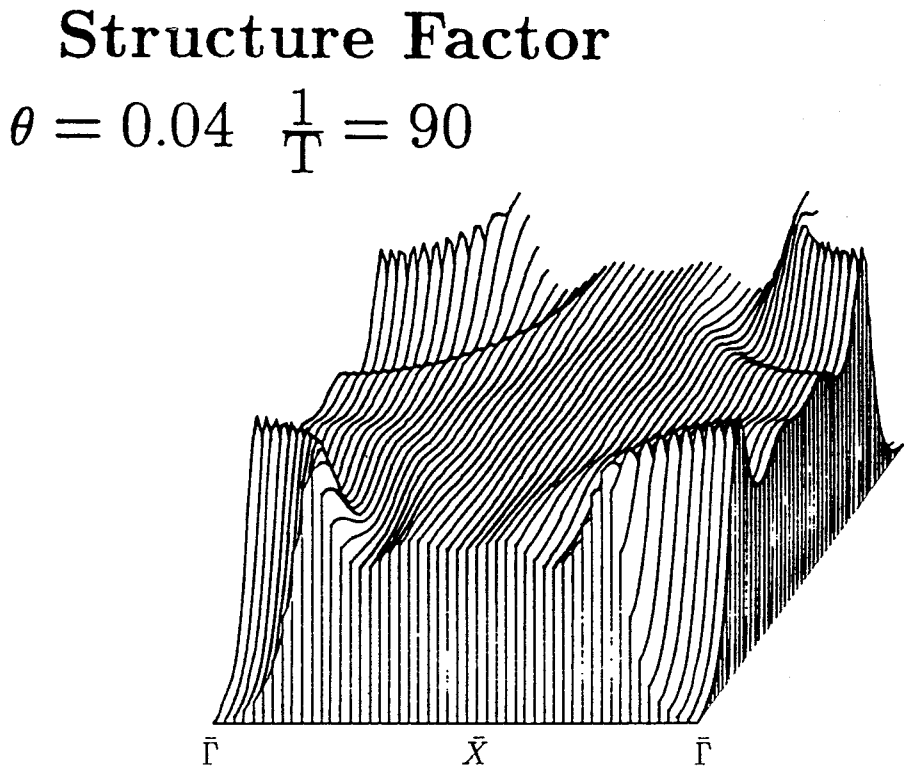

Figure 2.3: The stereograph of the structure factor

The structure fuctor is calculated at $\theta = 0.04$ and $\beta(\equiv \frac{1}{T}) = 90$. The stereograph is drawn on the unit cell of the reciprocal lattice.

range order is appreciable. Of course the adsorbate cannot move on the surface, that is, surface diffusion stops at some lower temperatures so that the numerical results at the low temperature may not be observed experimentally.

The coverage dependence of the radius of this ring pattern is not so simple as $\theta^{1/2}$, which comes from the fictitious adsorbate lattice assumption[8][9], as is shown in Figure 2.4.

Average dipole interaction

The coverage dependence of the average local dipole interaction is calculated as shown in Figure 2.5-2.7. Each parameter of β corresponding to room temperature for Na(K) on Ni(100) or Cu(100) is shown in Table 2.2. In Figure 2.5-2.7, the EELS peak energies observed by the experiment[18][19] are shown. Their coverage dependence is may to reflect the average local dipole interaction. Those data points are $\log \Delta\omega_s$ as a function of $\log \theta$, where

$$\Delta\omega_s = \omega_s(\theta) - \omega_s(0)$$

and ω_s is the EELS peak energy. This excitation is understood as the electronic excitation from the conduction band states of the metal to the empty states, which is localized on the alkali metal adsorbate. If this empty state is constructed by the valence state of the alkali atom, the energy level of the adatom state has the coverage dependence coming from the average local dipole interaction.

The data points indicate that following relation holds, for $\theta \ll 1$.

$$\Delta\omega_s = A\theta^{\alpha},$$

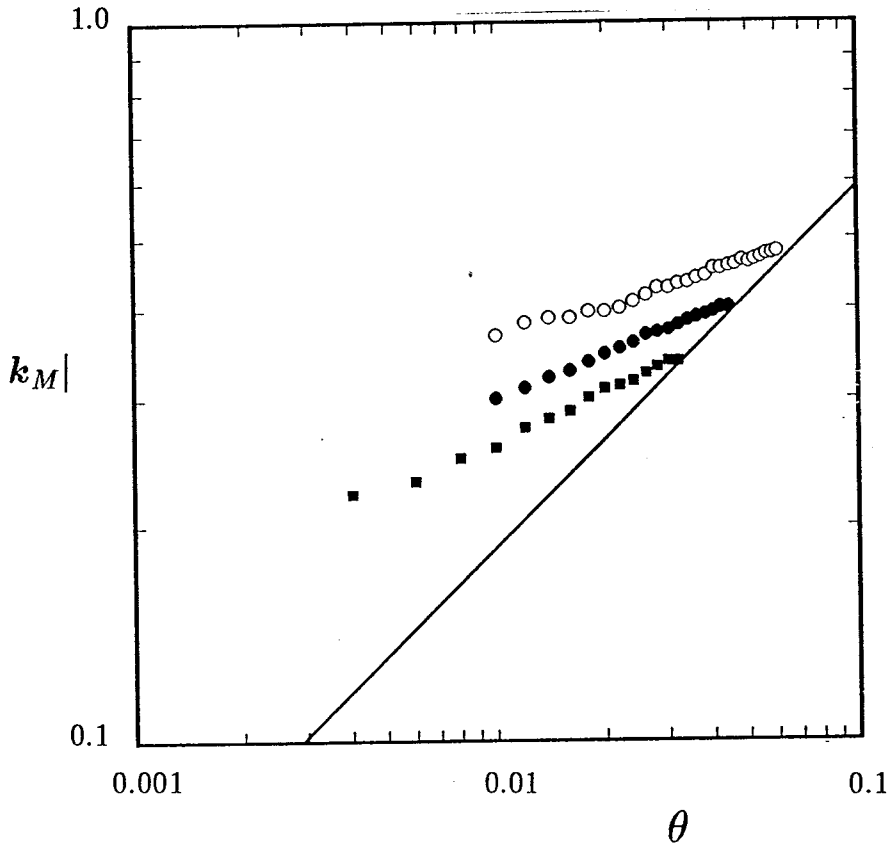

Figure 2.4: The coverage dependence of the radius of the diffuse ring

The radius of the diffuse ring, $|k_M|$, is ploted for the coverage, θ, on a log-log scale. Open circles, filled circles and filled box are repersenting the results of Na on Ni(100), K on Ni(100) and K on Cu(100), respectively. The solid line is given by $2\pi\sqrt{\sqrt{3}/2}\theta^{1/2}$, which comes from the fictitious adsorbate lattice assumption.

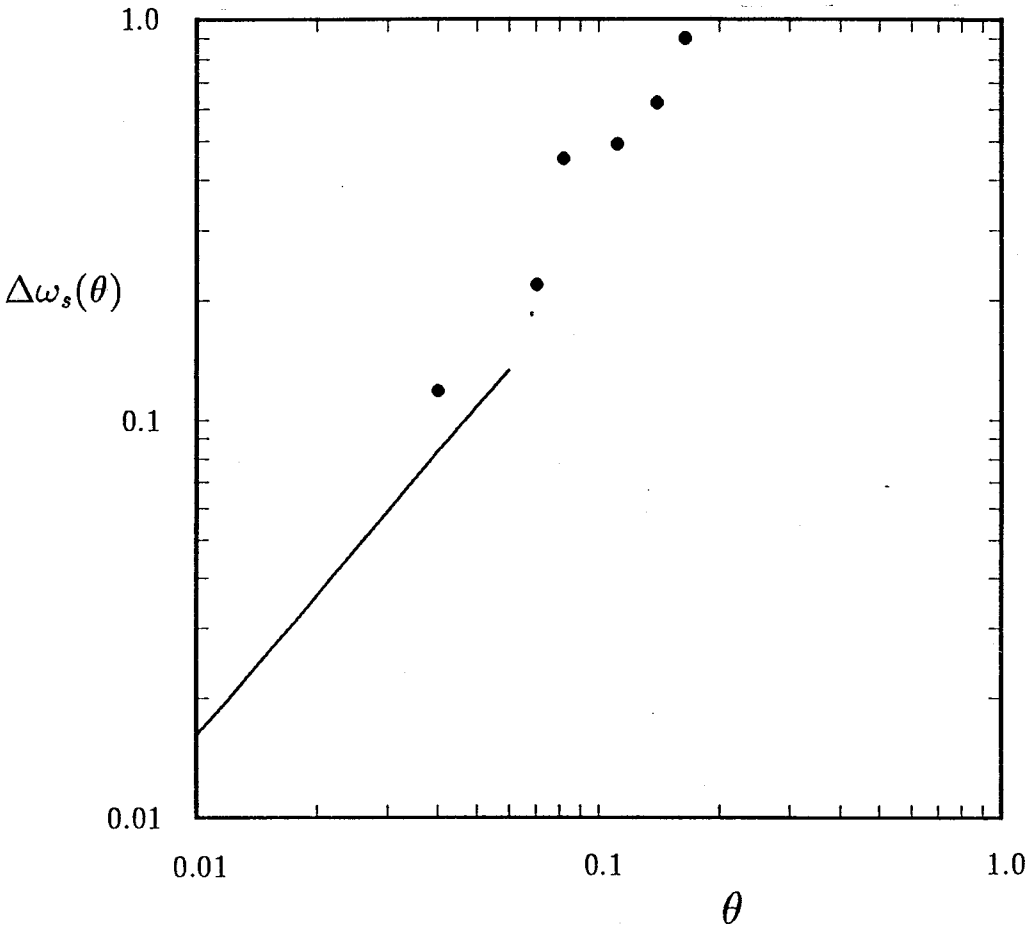

Figure 2.5: The EELS peak of Na on Ni(100)

Filled circles are experimental results obtained by [18] and the solid curve is the numerical calculation in this thesis. They are ploted on a log-log scale.

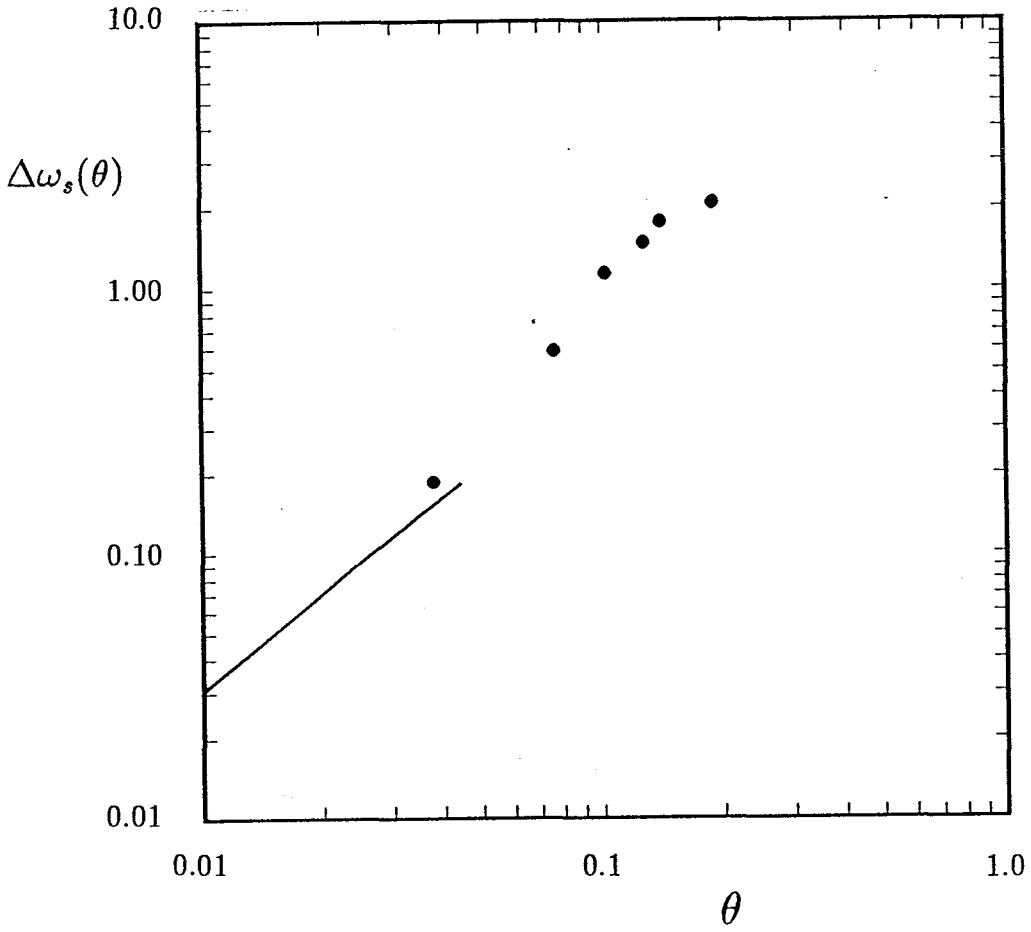

Figure 2.6: The EELS peak of K on Ni(100)

Filled circles are experimental results obtained by [18] and the solid curve is the numerical calculation in this thesis. They are ploted on a log-log scale.

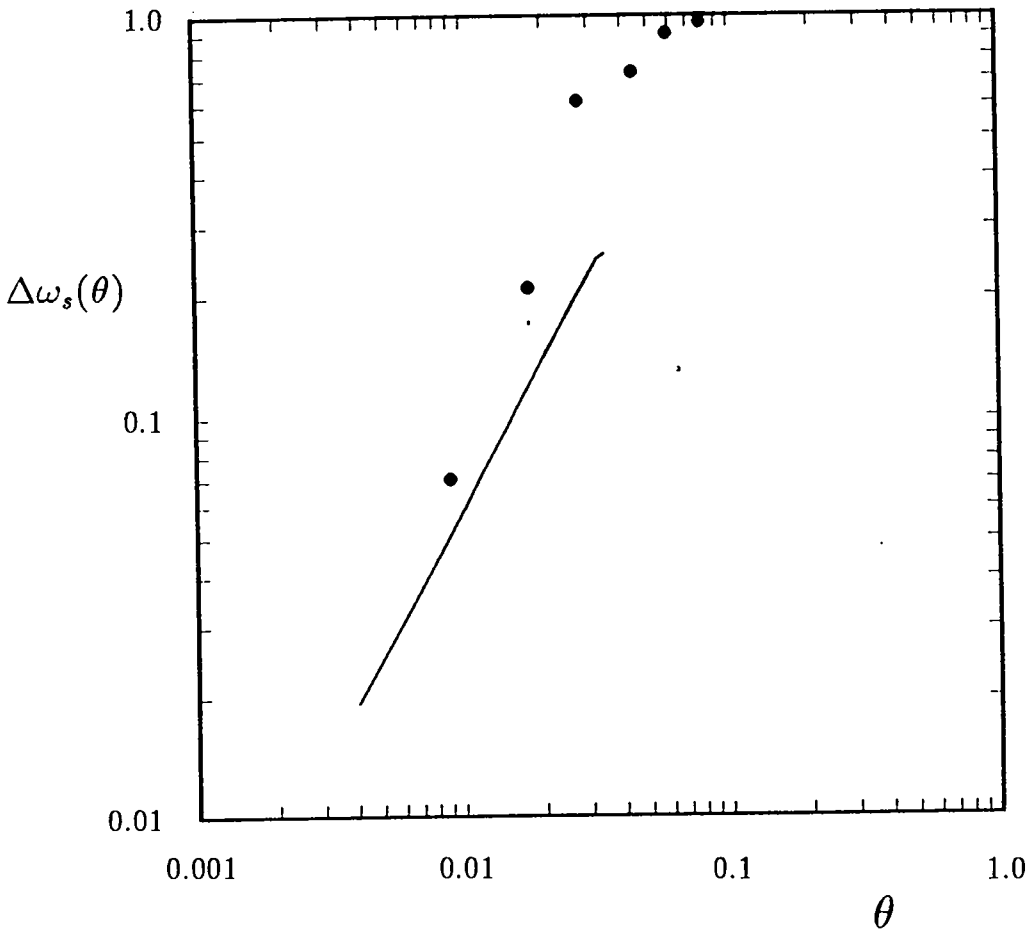

Figure 2.7: The EELS peak of K on Cu(100)

Filled circles are experimental results obtained by [19] and the solid curve is the numerical calculation in this thesis. They are ploted on a log-log scale.

where A is a certain coefficient and α is the exponent which is determined by the short range order. The calculated results show a similar relation,

$$\sum_j J_{ij} \frac{\langle n_i n_j \rangle}{\theta} = A' \theta^{\alpha'},$$

for $\theta \ll 1$.

α' is not the simple value of 3/2, which comes from the fictitious adsorbate lattice assumption[8][9], or 1, which comes from the mean field theory, but the value between 1 to 1.5. If we assume that the coverage dependence comes from the average local dipole interaction and the alkali adsorbate is ionized completely, this numerical result can be compared with the experimental results without any adjustable parameter.

The coverage dependence of calculated local dipole interaction and its absolute value are in agreement with ones of the EELS peak obtained experimentally. Of course it is too early to say that this mechanism is the origin of coverage dependence of the EELS peak. There are several assumptions to relate these two quantities. For example, we do not quite understand the excitation process, which gives the EELS peak. This dipole field is also claimed to be in question at higher coverages by the recent calculation[2].

Diffuse LEED

The structure factor gives us some information to discuss the defuse LEED pattern. However, the dynamic form factor is needed for completely analysis of the defuse LEED pattern.

Recently, Kawamura [22] calculated the dynamic form factor of this system for

several distances between an alkali atom and metal atoms and the symmetric adsorbate sites, which are the on top, the bridge and the four fold hollow site at lower coverages where adsorbates do not interact each other. The LEED intensity, $I(k)$ is obtained as the structure factor multiplied by the dynamic form factor. They are shown in Figure 2.8-2.10. The stereograph of the dynamic factor shows a complex structure in the reciprocal lattice. The stereographs of the LEED intensity for certain parameters and adsorbate sites are shown in Figure 2.8-2.10. Some of stereographs show a clear ring pattern but others does not. One can find that the LEED pattern is very sensitive to a position of adsorbate. In the case that the dynamic form factor enhances the structure factor, the LEED pattern is determined mainly by the structure factor and the ring pattern will be observed. But when the effects of both the dynamic form factor and the structure factor compensate each other, LEED shows a very complex pattern determined by the dynamic form factor. The structure factor plays the role like a filter or a window for the dynamic form factor. The analysis of defuse LEED patterns by these numerical results of the correlation function combined with the dynamic form factor may determine the local structure of the surface system though it may be difficult to observe the diffuse LEED pattern with the required accuracy at lower coverages by the theoretical calculations.

The structure factor obtained here can be more easily compared with the diffuse pattern of X-ray diffraction because the kinematical analysis with simpler form factors is enough. Experimental studies of the diffuse diffraction for this system by use of SR(syncrotron radiation) X-ray are anxiously expected in future.

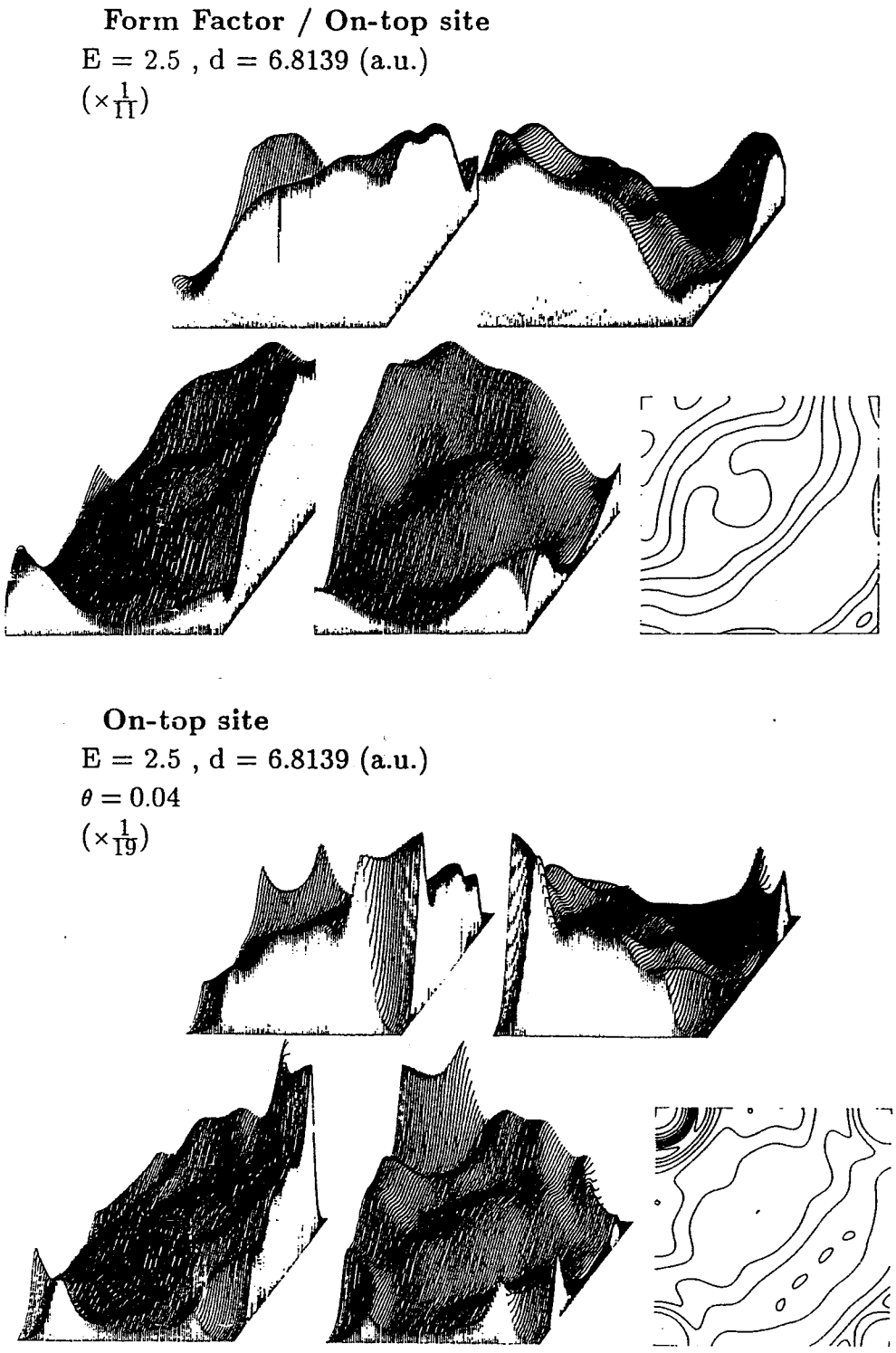

Figure 2.8: The stereograph of diffuse LEED intensity I

The calculation are made at $\theta = 0.04$ and T=300K, for the on top site of K on Ni(100). The stereographs are drawn on the four unit cells and the contour map is draw on the unit cell of the reciprocal lattice around (0,0), where each corner corresponds to (0,0) point. E(eV) is the energy of the incident electron beam and 'd' is the distance between adsorbate and the metal surface.

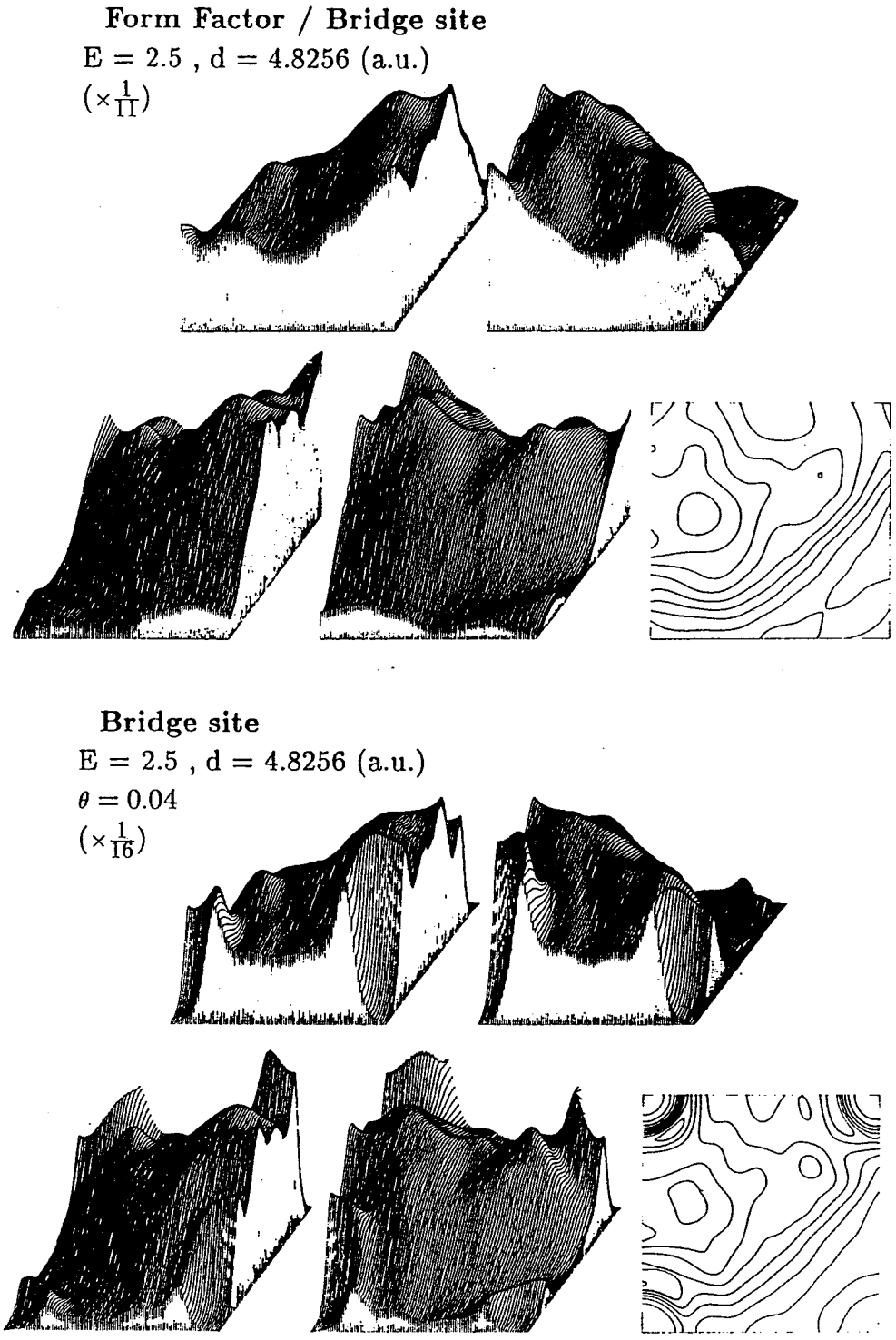

Figure 2.9: The stereograph of diffuse LEED intensity II

Same as in Figure 2.8. The calculation are made at $\theta = 0.04$ and T=300K, for the bridge site of K on Ni(100).

Form Factor / 4-fold hollow site
E = 2.5 , d = 5.2141 (a.u.)
($\times\frac{1}{34}$)

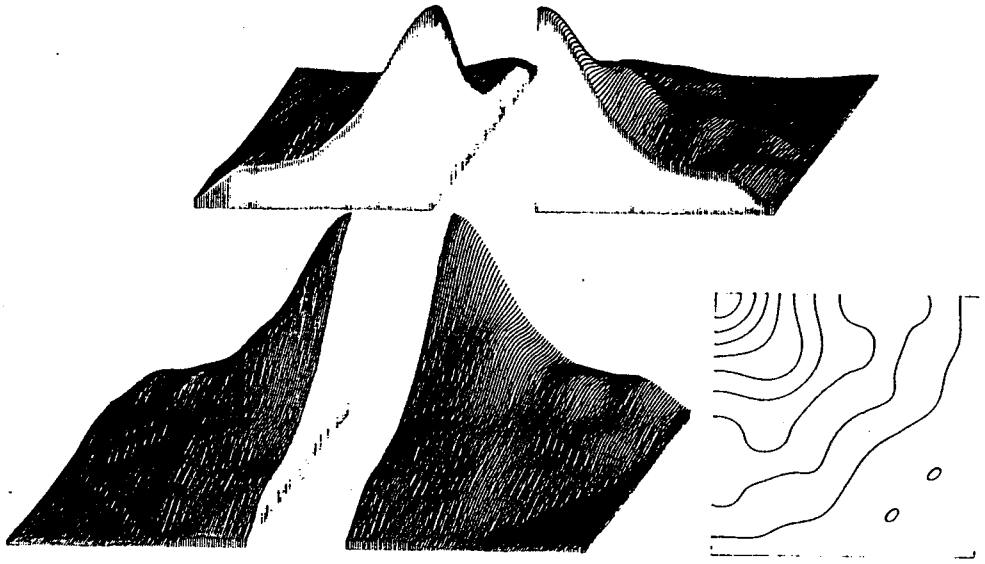

4-fold hollow site
E = 2.5 , d = 5.2141 (a.u.)
$\theta = 0.04$
($\times\frac{1}{27}$)

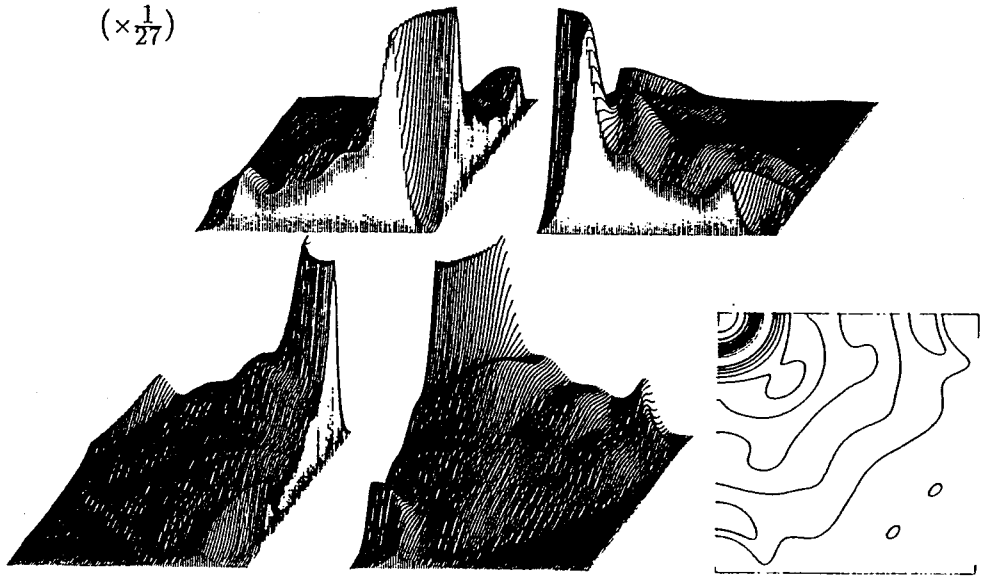

Figure 2.10: The stereograph of diffuse LEED intensity III

The calculation are made at $\theta = 0.04$ and T=300K, for the four fold hollow site of K on Ni(100).

2.3 Monte Carlo study

The solution of the set of integral equations(2.19) in previous section can be considered as that of the infinite system within the accuracy of the numerical calculation. However, it is valid only at low coverages and high temperatures. The computer simulation with the Monte Carlo method has no such a limitation about temperatures and coverages, although it can calculate the properties only in the finite system. One has to make the finite scaling procedure to obtain the infinite system results. The results in this section are preliminary. We need more extensive investigations to reach definit conclusions.

2.3.1 Model and method

The computer simulation of the alkali adsorbate system is made by Monte Carlo method. The square lattice gas model is used for computer simulation as in the previous section. The Hamiltonian is given by (2.1). The system is treated as the canonical ensemble. Its sampling are performed by the Metropolis important sampling algorithm. The longer potential range of the dipole-dipole interaction also makes this calculation very difficult. We consider an $n \times n$ finite system and use the periodic boundary condition. And we put enough number of $n \times n$ systems around the central $n \times n$ system which is the object of sampling, in order to get the convergent summation of the dipole-dipole interaction.

2.3.2 Size effect of the correlation function

The simulation is made for the several system size, 20×20, 25×25 and 30×30 at the temperature corresponding to the room temperature of K/Ni(100). The ensemble average are given as the average over 3000 Monte Carlo steps after discarding first 3000 steps.

The correlation function along the x is shown in Figure 2.11. They agree with the solution of (2.19) qualitatively but not quite quantatively. They are not smooth and somewhat unnatural compared with the results in the previous section probably because of effects due to the periodic boundary condition. This trend is more remarkable in the larger system. This may be partly because the number of sampling Monte carlo steps is very small. We have to take more sampling points as the phase space of larger even with important sampling algorithm. Particularly the correlation function needs more sampling points than the energy of the system needs.

Then the results for the 20×20 system agree with the solution of (2.19) rather than those of the larger systems. It is not smooth but is in agreement, with respect to the peak or dip positions and with the results from the high temperature expansion.

These results indecates a hope that we can discuss this type of the systems, which has the dipole-dipole interaction, by the Monte Carlo method. The Monte Carlo simulation is expected to be useful at high coverage and low temperature regions where the high temperature expansion is not valid. In such a high coverage region, not only the dipole-dipole interaction but the short range interaction between alkali metal atoms with an electronic origin may be also needed to explain the experimental results[19].

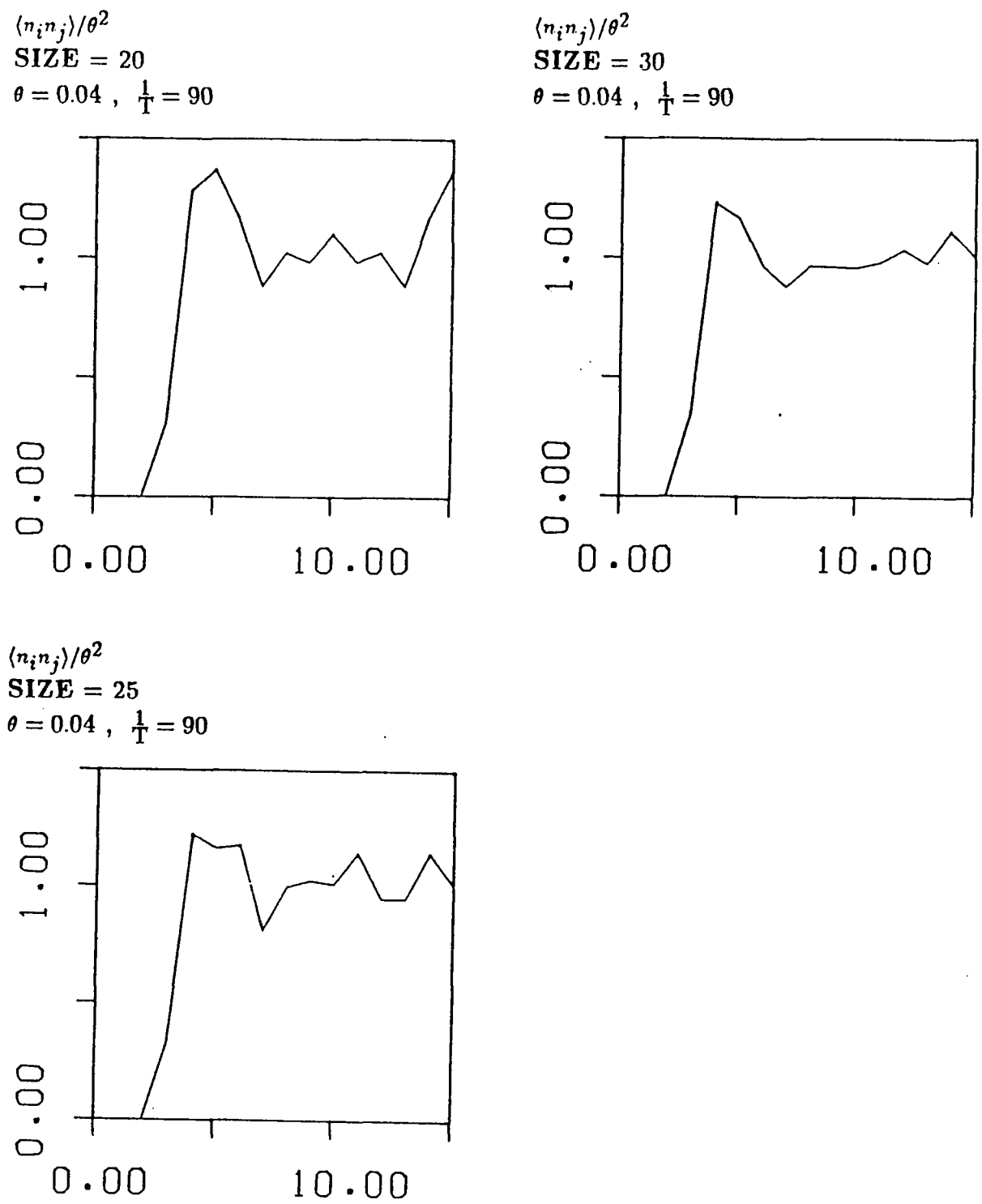

Figure 2.11: Size dependence of correlation function

The correlation function divided by θ^2 along $\langle 10 \rangle$ direction

2.4 Discussion

2.4.1 Temperature Green function

The diagramatical perturbation theory of Green function is also useful to obtain the self-consistent effective interaction of lattice gas system as well as high temperature expansion method. Here we have the Hamiltonian as follows,

$$\mathcal{H} = \frac{1}{2}\sum_{ij} J_{ij} a_i^\dagger a_i a_j^\dagger a_j - \mu \sum_i a_i^\dagger a_i, \tag{2.24}$$

where $a_i^\dagger$ and a_i are creation and annihilation operator of particles on i site on the lattice. These operators satisfy the commutation relation of the Fermi operator,

$$\{a_i, a_j^\dagger\} = a_i a_j^\dagger + a_j^\dagger a_i = \delta_{ij}, \tag{2.25}$$

$$\{a_i^\dagger, a_j^\dagger\} = 0, \tag{2.26}$$

$$\{a_i, a_j\} = 0, \tag{2.27}$$

and it is reasonable because two or more adsorbates cannot occupy the same adsorption site. The Fermi statistics does not affect results, because $\mathcal{H}$ does not contain the particle transfer term. The one particle Green function is defined by

$$G_i(\tau, \tau') = \langle \mathrm{T} a_i(\tau) a_i^\dagger(\tau') \rangle, \tag{2.28}$$

where $a_i(\tau)$ and $a_i^\dagger(\tau)$ are annihilation and creation operators in the Heizenberg representation on the i-th site. The particle density which means a coverage can be obtained as

$$\langle n_i \rangle \equiv \theta = \lim_{\tau' \to \tau + 0^+} G_i(\tau, \tau'). \tag{2.29}$$

We take the first term of (2.24) as the perturbation. The perturbation expansion of Green function can be described by Fymann's diagram as follows.

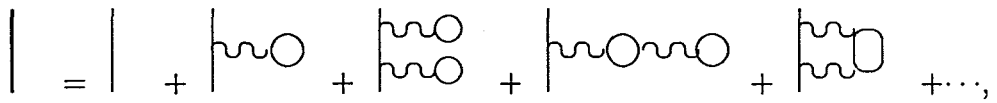

where the broad and fine solid line are corresponding to the Green function, $\mathcal{G}_i(i\omega_\ell)$, and the unperturbed Green function, $\mathcal{G}_i^{(0)}(i\omega_\ell)$, respectively. They are defined as

$$G_i(\tau,\tau') = \frac{1}{\beta}\sum_\ell \mathcal{G}_i(i\omega_\ell)e^{-i\omega_\ell(\tau-\tau')}, \tag{2.30}$$

$$G_i^{(0)}(\tau,\tau') = \frac{1}{\beta}\sum_\ell \mathcal{G}_i^{(0)}(i\omega_\ell)e^{-i\omega_\ell(\tau-\tau')}, \tag{2.31}$$

particularly, $\mathcal{G}_i^{(0)}(i\omega_\ell)$ is obtained as,

$$\mathcal{G}_i^{(0)}(i\omega_\ell) = \frac{1}{i\omega_\ell+\mu}, \tag{2.32}$$

where $\omega_\ell = \dfrac{(2\ell+1)\pi}{\beta}$ and $\ell = 0, \pm1, \pm2, \cdots$.

Each diagram corresponds to each perturbation term and follows Fymann's rule in the lattice space with the Fourier transform of the imaginary time except for following modifications.

1. Label each vertex with a internal site index.

2. The wavy line is corresponding to J_{ij}.

3. Sum up all internal site indices over lattice.

4. ω_ℓ conserves at each vertex.

These diagrams have one to one correspondence to the graphs of high temperature expansion. The *end* with n interaction lines and the *joint* of $n+1$ interaction lines correspond to $n+1$ external lines of unperturbed Green functions with the

same site index or a ring of $n+1$ internal lines of unperturbed Green functions with same site index, respectively. On the limit of $\tau' \to \tau + 0^+$, the both of them are corresponding to function F_n obtained as,

$$F_n = n!\frac{(-1)^n}{\beta^n}\sum_{\ell}\left(\mathcal{G}_i^{(0)}(i\omega_\ell)\right)^{n+1}, \tag{2.33}$$

$$= n!\frac{(-1)^n}{\beta^n}\frac{1}{2\pi i}\oint\left(\mathcal{G}_i^{(0)}(\omega)\right)^{n+1} f(\omega)d\omega, \tag{2.34}$$

where $f(\omega)$ is the Fermi distribution function defined by

$$f(\omega) = \frac{1}{\exp\{\beta\omega\}+1}.$$

The coefficient, $n!$ indicates that this sort of diagram have $n!$ topological equivalent diagrams.

F_n can be described with the chemical potential as follows,

$$F_n = n!\frac{(-1)^n}{\beta^n}\Im\int_{-\infty}^{\infty} d\omega\frac{f(\omega)}{(\omega+\mu)^{n+1}}, \tag{2.35}$$

$$= \frac{(-1)^n}{\beta^n}\Im\int_{-\infty}^{\infty} d\omega\frac{f^{(n)}(\omega)}{\omega+\mu}, \tag{2.36}$$

$$= \frac{(-1)^n}{\beta^n}f^{(n)}(-\mu), \tag{2.37}$$

where $f^{(n)}(\omega)$ means the n-th derivative respect to ω. By use of $c = f(-\mu)$, we can obtain the same relation of (2.13).

Two particle Green function describing two particle correlation function is defined as

$$g_{ij}(\tau,\tau') = \langle \mathrm{T} n_i(\tau) n_j^\dagger(\tau')\rangle, \tag{2.38}$$

where n_i is the number operator of ith site. Two particle correlation function is obtained by

$$\langle n_i n_j\rangle = \lim_{\tau'\to\tau+0^+} g_{ij}(\tau,\tau'). \tag{2.39}$$

The perturbation expansion of two particle Green function can also performed by use of previous rule as follows,

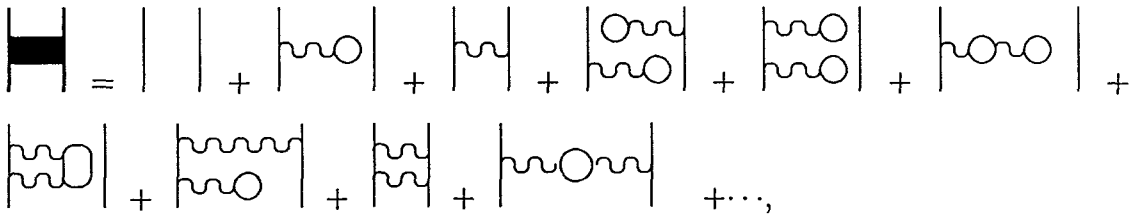

where the diagram of the left hand side of this diagramatical equation corresponds to the two particle Green function.

All internal lines and interaction lines which are not connected with external lines and other internal lines, can be renormalized to exact Green function. The two particle Green function can be expanded as follows by use of the exact Green function.

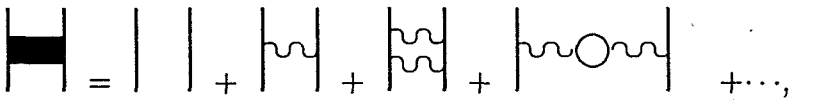

where thick solid lines are representing exact one particle Green function. In this case, the unperturbed Green function does not depend on the site index, so we can take the limit of $\tau' \to \tau + 0^+$ on each site independently. Those diagramatical expression is the same as the expression of the high temperature expansion within the approximation,

$$\int_{-\infty}^{\infty} \mathcal{G}(\omega)^2 f(\omega) d\omega \sim \theta. \tag{2.40}$$

2.4.2 Kirkwood method

The set of integral equations for the effective interaction obtained from the high temperature expansion can be also derived by a lattice version of the Kirkwood

method[23]. Kirkwood applied this method for liquid and gas systems to obtain effective field. We apply the same procedure as the Kirkwood method for the lattice gas system.

We consider the lattice gas system including $N+1$ particles. The lattice has M sites where particles can sit on. Treating this system in the canonical ensemble, the coverage, θ, is obtained by

$$\theta = \frac{N+1}{M}. \tag{2.41}$$

According to the Kirkwood method, Hamiltonian of this system is defined by

$$\mathcal{H}(\xi) = \xi \sum_{i=1}^{N} J(r_i - r_0) + \sum_{i>j\geq 1}^{N} J(r_i - r_j), \tag{2.42}$$

where r_i is the position vector of the i-th particle on the discrete lattice, and $J(r_i - r_j)$ is the interaction between the i-th particle and the j-th particle. Particularly the potential between the zeroth particle and the other particles is multiplied by a parameter ξ. So $\xi = 1$ corresponds to the $N+1$ particles system and $\xi = 0$ corresponds to the N particles system. The summation of $r_0, r_1, \cdots, r_N$ runs over M lattice sites excluding the sites that another particles already sit on.

The conditional probability, $\mathcal{P}_0(r_1 : \xi)/M$ that the first particle sits on the r_1 site when the zeroth particle sits on the r_0 site, is obtained by

$$\mathcal{P}_0(r_1 : \xi) = \frac{\sum_{r_2, r_3 \cdots r_N}^{M} e^{-\beta\mathcal{H}(\xi)}}{\sum_{r_1, r_2 \cdots r_N} e^{-\beta\mathcal{H}(\xi)}}. \tag{2.43}$$

An effective interaction is defined from the conditional probability as follows,

$$\mathcal{P}_0(r_1 : \xi) \equiv \exp[-\mathcal{J}(r_1 : \xi)], \tag{2.44}$$

where we put r_0 onto the origin. The particle sitting on r experience the mean effective interaction, $\mathcal{J}(r:\xi)$, from the particle sitting on the origin. Thus $\mathcal{J}(r:\xi)=0$ for $\xi=0$, and we denote $\mathcal{J}(r:\xi)=\mathcal{J}(r)$ for $\xi=1$.

The differential equation of $\mathcal{J}(r:\xi)$ is obtained by

$$\frac{\partial \mathcal{J}(r_1:\xi)}{\partial \xi} = \sum_{r_2,r_3,\cdots,r_N} \frac{\sum_{i=1}^{N} \beta J_{0i} e^{-\beta \mathcal{H}(\xi)}}{\sum_{r_2,r_3,\cdots,r_N} e^{-\beta \mathcal{H}(\xi)}} - \sum_{r_1,r_2,\cdots,r_N} \frac{\sum_{i=1}^{N} \beta J_{0i} e^{-\beta \mathcal{H}(\xi)}}{\sum_{r_1,r_2,\cdots,r_N} e^{-\beta \mathcal{H}(\xi)}}$$

$$= \beta J_{01} + \frac{N-1}{M-1} \sum_{r_2} \beta J_{02} \mathcal{P}_{01}(r_2:\xi) - \frac{N}{M} \sum_{r_2} \beta J_{02} \mathcal{P}_0(r_2:\xi), \qquad (2.45)$$

where $\mathcal{P}_{01}(r_2:\xi)$ in (2.45) is the conditional probability that the second particle sits on the r_2 site, when the zeroth and first particle sit on the r_0 and the r_1 sites, respectively. $\mathcal{P}_{01}(r_2:\xi)$ is related to the three particle correlation function and defined by

$$P_{01}(r_2:\xi) = \frac{(M-1) \sum_{r_3,r_4,\cdots,r_N} J_{0i} e^{-\beta \mathcal{H}(\xi)}}{\sum_{r_2,r_3,\cdots,r_N} e^{-\beta \mathcal{H}(\xi)}}. \qquad (2.46)$$

Here we apply an approximation of superposition to $\mathcal{P}_{01}(r_2:\xi)$ as follows,

$$\begin{aligned} \mathcal{P}_{01}(r_2:\xi) &\approx \mathcal{P}_0(r_2:\xi) \cdot \mathcal{P}_1(r_2:\xi=1) \\ &\approx \exp[-\mathcal{J}(r_2:\xi)] \exp[-\mathcal{J}(r_2-r_1)]. \end{aligned} \qquad (2.47)$$

This would be a good approximation at low coverages.

In the limit of $N \to \infty$ and $M \to \infty$ with keeping θ constant, (2.45) becomes

$$\frac{\partial \mathcal{J}(r_1:\xi)}{\partial \xi} = \beta J(r_1) + \beta\theta \sum_{r_2} J(r_2) e^{-\mathcal{J}(r_2:\xi)} (e^{-\mathcal{J}(r_2-r_1)} - 1). \qquad (2.48)$$

Integrating over ξ (2.48) with use of $\mathcal{J}(r:\xi=0)=0$, we get

$$\mathcal{J}(r_1:\xi) = \beta J(r_1)\xi + \beta\theta \sum_{r_2} \mathcal{L}(r_2-r_1) J(r_2) \int_0^{\xi} e^{-\mathcal{J}(r_2:\eta)} d\eta, \qquad (2.49)$$

where $\mathcal{L}(r) = e^{-\mathcal{J}(r)} - 1$, which is the same definition of $\mathcal{L}(r)$ in previous section(2.2.5) The integral in (2.49) is rewritten by integration by parts over η in (2.49) and use of (2.48) and (2.49) itself as ,

$$\begin{aligned}
&\beta J(r_1) \int_0^\xi e^{-\mathcal{J}(r_1:\eta)} d\eta \\
&\quad = -\int_0^\xi e^{-\mathcal{J}(r_1:\eta)+\beta J(r_1)} \frac{d}{d\eta} e^{-\beta J(r_1)} d\eta \\
&\quad = -\mathcal{L}(r_1 : \xi) - \beta\theta \sum_{r_2} \mathcal{L}(r_2 - r_1) J(r_2) \int_0^\xi d\eta e^{-\mathcal{J}(r_1:\eta)} e^{-\mathcal{J}(r_2:\eta)}, \qquad (2.50)
\end{aligned}$$

where $\mathcal{L}(r : \xi) = e^{-\mathcal{J}(r:\xi)} - 1$.

(2.49) and (2.50) can be rewritten by the Fourier transformation as

$$\mathcal{J}(k) = \beta J(k) + \theta \mathcal{L}(k) \Gamma(k), \qquad (2.51)$$

$$\Gamma(k) = -\mathcal{L}(k) - \theta \mathcal{L}(k) \Gamma(k) - \theta \Delta(k), \qquad (2.52)$$

where $\mathcal{J}(k)$, $\mathcal{L}(k)$ and $J(k)$ are Fourier components of $\mathcal{J}(r)$, $\mathcal{L}(r)$ and $J(r)$, respectively. $\Gamma(k)$ and $\Delta(k)$ are defined as,

$$\Gamma(k) = \sum_{\mathbf{r}} e^{ikr} \beta J(r) \int_0^1 e^{-\mathcal{J}(r:\xi)} d\xi, \qquad (2.53)$$

$$\Delta(k) = \sum_{r,\, r'} e^{ikr} \int_0^1 d\xi \beta J(r') e^{-\mathcal{J}(r':\xi)} \mathcal{L}(r' - r) \mathcal{L}(r : \xi). \qquad (2.54)$$

$\Gamma(k)$ can be written as

$$\Gamma(k) = -\frac{\mathcal{L}(k)}{1 + \theta \mathcal{L}(k)} - \theta \frac{\Delta(k)}{1 + \theta \mathcal{L}(k)}. \qquad (2.55)$$

Then $\mathcal{J}(k)$ is obtained by use of (2.52) and (2.55) as

$$\mathcal{J}(k) = \beta J(k) - \frac{\theta \mathcal{L}(k)^2}{1 + \theta \mathcal{L}(k)} - \frac{\theta^2 \mathcal{L}(k) \Delta(k)}{1 + \theta \mathcal{L}(k)}. \qquad (2.56)$$

Table 2.3: Error estimation of Kirkwood method

β	θ	ε
40	0.04	-8.102×10^{-3}
90	0.02	-9.123×10^{-3}
90	0.04	3.592×10^{-2}

We have the first iteration to the right hand side of (2.52) as $-\beta\theta \sum_2 \mathcal{L}_{12}\mathcal{L}_{02}\mathcal{L}_{01}$, where we assume that $cJ_{02}(\eta) \approx \mathcal{J}_{02}(0)\cdot\eta$, $\mathcal{J}_{02} \approx J_{02}$ and $\mathcal{L}_{02}(\eta) \approx \mathcal{L}_{02}(1)$. The estimated error, ε, is defined by the ratio of the summation of the third term over k to the summation of second term of the right hand side of (2.52).

By neglecting the third term of the right hand side of (2.56), we can obtain the same equation as the equation obtained from high temperature expansion. This approximation may be good when θ is very small.

Using the solution in section 2.2.5, we can estimate the error due to the neglected term. The third term of the right hand side of (2.56) is estimated as order of 10^{-2} of second term at $\beta = 40$, $\theta = 0.04$ and $R_c = 60a_0$, so that our approximation may be good. However the approximation becomes poor at further low temperatures even at lower coverages as we notice from Table (2.3).

2.5 Conclusion

The correlation function of alkali metal adsorbates on the metal surface was obtained from a set of approximate but plausible integral equations at lower coverages and higher temperatures without any adjustable parameter. It shows temperature and coverage dependence, which seems quite reasonable. We believe that the present

set of integral equations provides a reasonable approximation for the dilute dipole-dipole repulsive systems in the two dimension. The coverage dependence of the average local dipole interaction was obtained from the calculated correlation function. Traditionally, it is considered that this property relates the peak of EELS spectra. Muscat and Newns[8][9] explained this coverage dependence of EELS peak by the assumption of a fictitious adsorbate lattice incommensurate to the substrate before. However in fact, no long range order has been observed by LEED at coverages and temperatures where EELS were measured. We got a good agreement with the coverage dependence of the EELS peak with short range order but without long range order. If the system shows diffuse ring patterns whose diameter depends coverage, then it would be likely that this mechanism has some contribution to the EELS peak excitation, although physical picture of this excitation is not clear. This system has a very strong short range order caused by the existence of dipole-dipole interaction which extends to longer distance.

The coverage dependence of the diameter of the ring pattern of LEED is discussed. This is also explained by the short range order. We got more natural dependence than one which had been obtained by a fictitious lattice before. We can get the realistic diffraction image theoretically by the combination of the structure factor calculated by this method and the dynamic form factor obtained by Kawamura[22]. Unfortunately, our method to calculate the correlation function is valid at lower coverages. The ring pattern has not been observed by LEED at such a low coverage yet. But the comparison of the diffuse ring pattern obtained by the experiment and the calculation must give much information about the adsorbates,

if such a measurement is possible.

The computer simulation for the dipole-dipole interaction system is examined preliminarily. It is found that one has to construct an appropriate finite size scaling method.

Chapter 3

Asymmetric dimer on Si(100) surface

3.1 Phase Transition on Si(100)

The Si(100) surface has the (2×1) reconstruction at the room temperature, and undergoes the phase transition at about 200K[24]. The low temperature phase has the c(4×2) structure. It is believed that the c(4×2) structure is the ordered state of asymmetric dimers, which is proposed by Yin and Cohen[25]. Two sorts of asymmetric dimers which have opposite directions of asymmetry each other are arrayed alternately in the c(4×2) structure like an antiferromagnetic Ising spin system.

For the (2×1) phase, several possible structures have been considered. The symmetric dimers system, the *ferro* magnetic like ordered structure of asymmetic dimers or the disordered state of asymmetic dimers can give the (2×1) diffractional structure.

3.1.1 Experimental results

Diffractional analysis

According to LEED by Kubota and Murata [26], a clear streak pattern is observed above the transition temperature. Weak streak patterns are observed even at 450K. The intensity of streak patterns is enhanced as the temperature decreases.

These streak patterns represent the short range order where dimers are arranged with twice periodicity of the substrate in each dimer row, however, dimer rows have little correlation each other down to a temperature region near the transition point. The quarter-ordered diffraction spots appear in the more enhanced streak pattern at 320K. At the temperature below about 200K, the c(4×2) structure is observed clearly.

These diffraction results indicate that the Si(100)2×1 surface has very strong *antiferro* correlation along the dimer row even at high temperatures and there exists the correlation between dimer rows only near the transition temperature.

Spectroscopic analysis

The surface electronic structure of Si(100)2×1 surface, particularly for the surface states consisting of dangling bonds of the dimers, is observed by angle resolved ultraviolet photoemission spectroscopy(ARUPS)[27]. The short range order in the dimer rows have an effect on the electronic structure of the dangling bonds of dimers.

Enta, Suzuki and Kono find that the photoelectron spectra change dramatically between 2×1 and c(4×2) along the $(\bar{\Gamma} - \bar{J})$ direction which is the direction perpendicular to the dimer rows. The surface Brillouin zone is shown in Figure 3.1. For

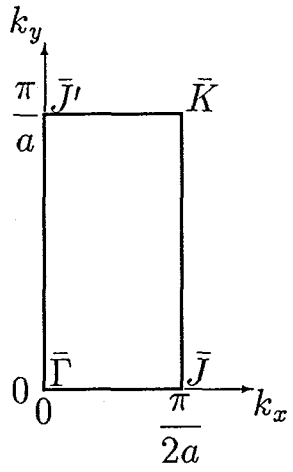

Figure 3.1: The surface Brillouin zone of Si(100)2×1 surface

the $(\bar{\Gamma} - \bar{J}')$ direction, which is parallel to the dimer rows, most of the electronic structure of c(4×2) are already observed even in the spectra of 2×1 surface.

These spectra of the surface states for 2×1 and c(4×2) surface are in agreement with an *ab initio* calculation for the c(4×2) structure by Zhu et al.[1], which is based on the asymmetric dimer model. The mixed spectra of 2×1 and c(4×2) are discussed theoretically by Inoue, Nakayama and Kawai[28]. In their model, the asymmetric dimers are arranged alternately like the antiferromagnetic spins in the dimer rows, that is, the well developed short range order is assumed even in the high temperature 2×1 structure.

STM and XPS results

The STM is a very powerful tool for the surface study. The topography of STM for Si(100) shows the image that is the arrangement of symmetric *dumbbells* with 2×1 periodicity in the terraces which are wide enough and have no defect[14], while it

shows the zig-zag arrangement of *dumbbells* near the step and near the regions of dark contrast considered as some defects like a missing dimer. The former image is in agreement with the symmetric dimer model and the latter one agrees with the asymmetric dimer model. So, apparently, the stational asymmetric dimer cannot explain the topography of STM.

This results, however, may be interpreted as the symmetric dimer is stable but not observed in the STM topographic image. That is to say, each asymmetric dimer flips its direction so fast that STM observes an average image of the asymmetric dimer. Near the step and some defects, the asymmetric dimer cannot flip so fast or at all by some mechanism.

Not only the topography of STM but the core level shift of spectra observed in soft X-ray photoemission spectroscopy(XPS) also questions the asymmetric dimer model[16]. If there are the asymmetric dimers on the Si(100) surface, Si atoms constructing a dimer must see two different environments and corresponding two surface peaks are expected in the core level photoemission. However, the XPS experiment shows only one surface peak. If this fact means that Si atoms on the surface have only one environment, it may favor the symmetric dimer model. Yamazaki and Cho[15] show that it is possible to be observed only one peak in the XPS spectrum because of a final state interaction effect, even for the asymmetric dimer model.

Of course the symmetric dimer model may be possible. However the model of this system will have to explain the LEED and UPS. It seems that the symmetric dimer model has not succeeded in explaining these experimental results yet. We believe that the asymmetric dimer model favors in this surface.

In this chapter, we try to discuss this reconstruction transition on the Si(100) surface focusing the short ranged order and the role of the dipole-dipole interaction on the basis of the asymmetric dimer model. It is difficult to determine the magnitude of this dipole moment formed by the polarization of the bonding charge on the asymmetric dimer, which is suggested by the *ab initio* calculation[1]. We made a very simple model including the dipole-dipole interaction as a parameter.

3.2 Monte Carlo study

3.2.1 Ising spin model

Each asymmetric dimer has two equivalent configurations, so it can be described by a Ising spin[29]. We consider the interacting Ising spins on the rectangular lattice whose lattice constants are a_0 and $2a_0$. In this model, the Ising spin may not represent only an asymmetric dimer itself but also a whole local structure with asymmetric dimer, for example it may include a lattice distortion of substrate atoms.

The Hamiltonian is given by

$$\mathcal{H} = \sum_{i,j} J_{ij} S_i S_j, \tag{3.1}$$

$$J_{ij} = J_{ij}^{(d)} + J_{ij}^{(s)}, \tag{3.2}$$

$$J_{ij}^{(d)} = \frac{\mu^2}{|\boldsymbol{r}_{ij}|^3}\left[1 - 3\cos^2\Theta_{ij}\right], \tag{3.3}$$

where μ is the dipole moment of an asymmetric dimer and $\boldsymbol{r}_{ij}$ is its position vector. J_{ij} is two spin interaction constant and consists of dipole-dipole interaction, $J_{ij}^{(d)}$, and the near neighbor interaction, $J_{ij}^{(s)}$, which represents short ranged interaction, for example, of an electronic origin and/or due to lattice distortion. Θ is the angle

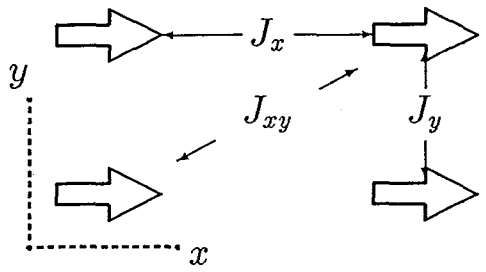

Figure 3.2: Geometrical arrangement of the interaction

between r_{ij} and the x-axis where the x-axis is taken perpendicular to the dimer rows as shown in Figure 3.2.

Then the ground state of the Ising spin system with only dipole-dipole interaction is the p(2×2) structure as seen in Figure 3.3. The potential surface, in the reciprocal space, of the dipole-dipole interaction is shown in Figure 3.4. In a model where the dipole-dipole interaction is dominant, the short range interaction of J_x, J_y and J_{xy} must be introduced to make the c(4×2) structure more stable than p(2×2) structure. The purpose of this analysis is to examine how the dipole-dipole interaction affects the detailed statistical properties of this system. To construct the computer simulation scheme for the dipole-dipole interaction system is another purpose of this work.

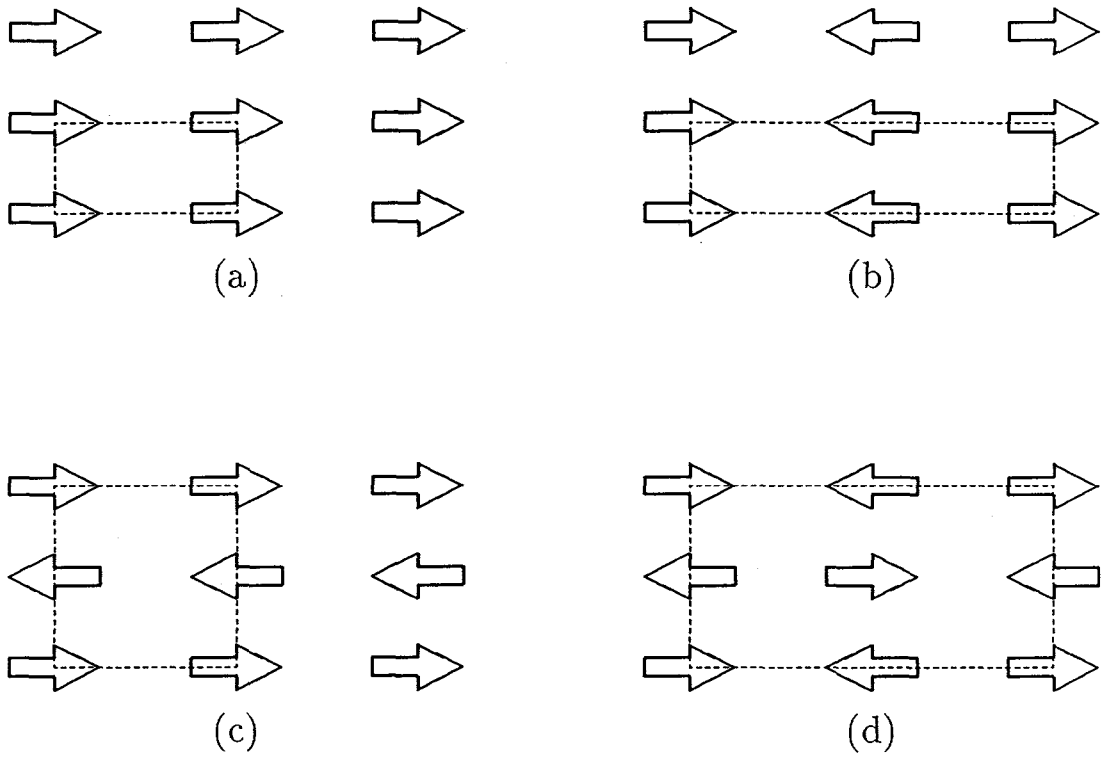

Figure 3.3: Possible ordered structure

(a):p(2×1), (b):p(4×1), (c):p(2×2), (d):c(4×2). The dashed lines show the unit cell of the reconstructed structure.

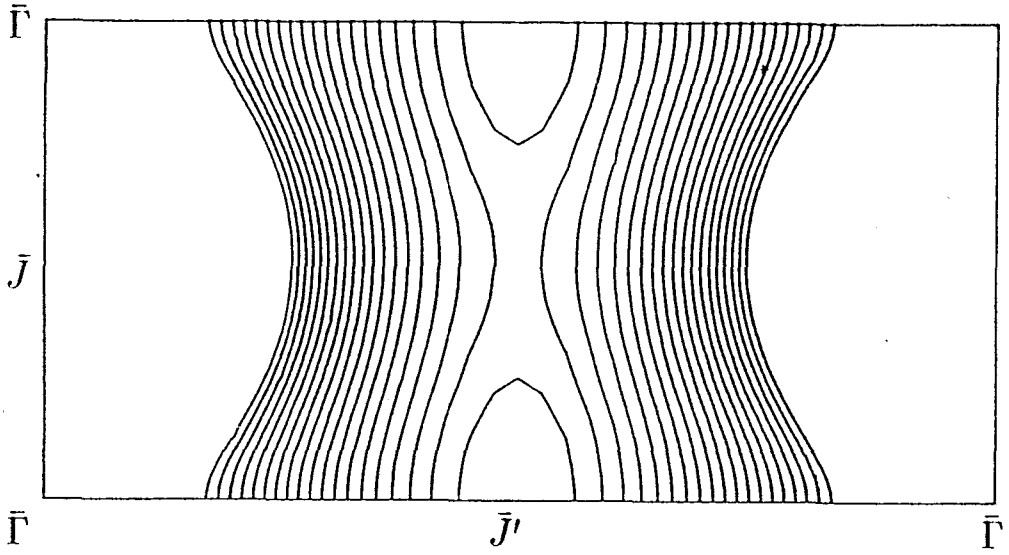

Figure 3.4: Potential surface of the dipole-dipole interaction

3.2.2 Computer simulation

The computer simulation is made by a Monte Carlo method. Its sampling is performed by the Metropolis important sampling algorithm. We consider an $n \times n$ finite system and use the periodic boundary condition. The dipole-dipole interaction extends its effect all over the finite system which is used by computer simulation. We put enough number of $n \times n$ systems around the central $n \times n$ system which is the object of sampling, in order to get the convergent summation of the dipole energy. For the units in the analysis we take $a_0 = 1$, $\mu = 1$ and $k_B = 1$ so that energy and temperature are measured in the unit of μ^2/a_0^3, but, in case of $\mu = 0$, we take $J_y = 1$, $a_0 = 1$ and $k_B = 1$ so that energy and temperature are in the unit of J_y. For the sake of comparisons, however, we take finally T_t as the unit of temperature and energy in each set of parameters.

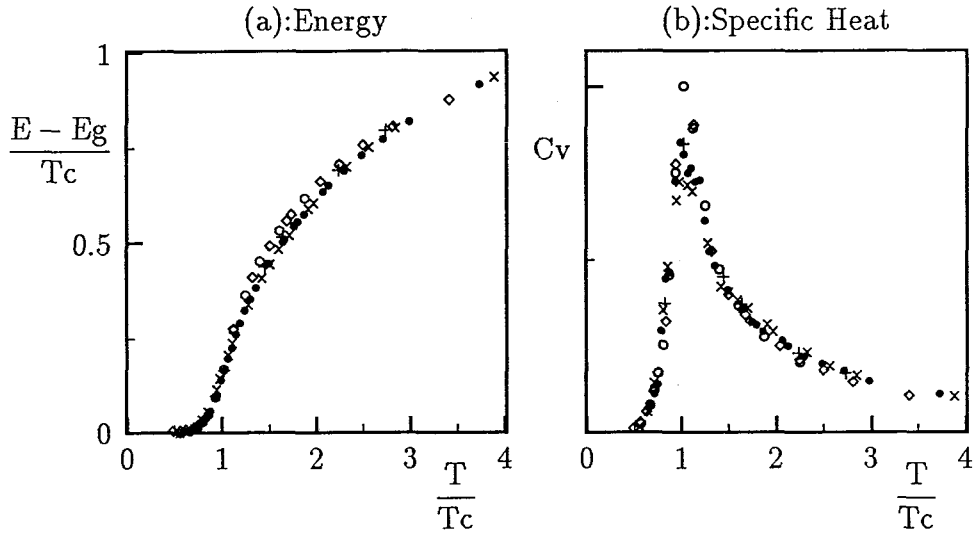

Figure 3.5: The temperature dependence of the energy and specific heat

Each symbol is introduced in Table 3.1

In this simulation, the system size is always 20×20 and most of values of ensemble average are given as the average over 10000—20000 Monte Carlo steps. The sampling starts from a snap shot which is determined at $T = 0.5$ and exclude first 5000–10000 Monte Carlo steps. This simulation is performed for several kinds of the interaction sets as in Table 3.1.

3.2.3 Energy and specific heat

Figure 3.5(a) and Figure 3.5(b) show the temperature dependence of the energy and the specific heat, respectively, for several parameter sets as shown in the Table 3.1(a). The temperature scale is normalized by the transition temperature, T_t, estimated by the peak temperature of the specific heat for each parameter set. The energy determined from the ground state energy, which is calculated numerically for

(a)

parameter set	J_x	J_y	J_{xy}	μ	symbol
(I) set	1.00	0.20	-0.15	1.00	$\bullet$
(II) set	1.00	0.20	-0.15	0.00	$\circ$
(III) set	1.00	0.05	0.00	0.00	$\times$
(IV) set	1.00	0.07	0.00	0.00	$+$
(V) set	1.00	0.10	0.00	0.00	$\diamond$

(b)

parameter set	J_x	J_y	μ	T_t	exact T_c
(s) set	-0.05	-1.0	0.0	0.76	0.74
(d) set	-0.075	0.0	1.0	0.64	—

Table 3.1: The parameter sets for the simulation

(a):The result for each parameter set is repersented in Figure 3.5 and 3.9 by the 'symbol' in this table.
(b):These two sets of the parameters have the same anisotropy in the sense discussed in the section 3.2.5.

the c(4×2) structure, is renormalized by T_t. Some snapshots are shown in Figure 3.6. The peak of the specific heat and the snapshots show the second order phase transition from the *para magnetic* 2×1 state to the *antiferro magnetic* c(4×2).

Both of the energy and the specific heat when temperatures are normalized by T_t have the similar behavior for any parameter chosen in this simulation. Of course this seems somewhat natural because the dipole-dipole interaction extends to longer distances but it is convergent in the two dimensional system. The system with the dipole-dipole interaction is considered to belong to the same universality class of the system with only the nearest neighbor interaction for the critical phenomena around the transition temperature. The specific heat shows the same behavior even outside of the critical region as that in the isotropic Ising system, which has very isotropic nearest neighbor interaction as shown in the Table 3.1(a). The T_t value for the (s) set can be estimated as 0.74 from the exact expression[30],

$$\sinh \frac{J_x}{k_B T_t} \sinh \frac{J_y}{k_B T_t} = 1.$$

The error by the finite size system of this computer simulation can be estimated by the comparison with this value and the value, 0.76, obtained by the simulation. It may not be very precise but may be enough for the discussion of the correlation function.

3.2.4 Correlation function

The two spin correlation function, $\langle S_i S_j \rangle$, is calculated for the parameter sets in the Table 3.1(a). The correlation function of the system with dipole-dipole interaction is shown in Figure 3.7 at several temperatures. When T_t is assumed about 200K

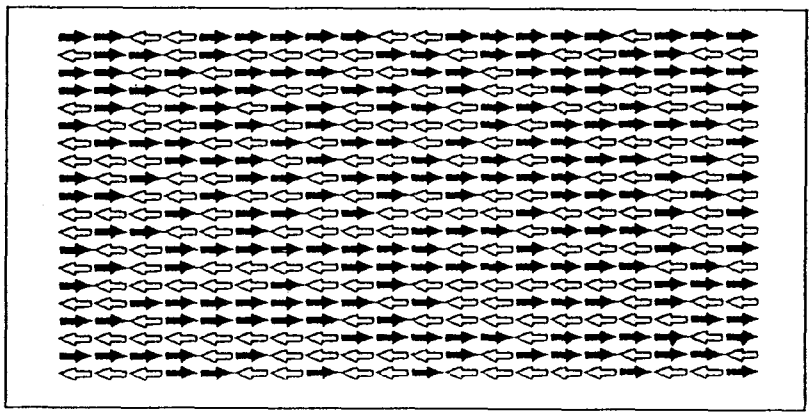

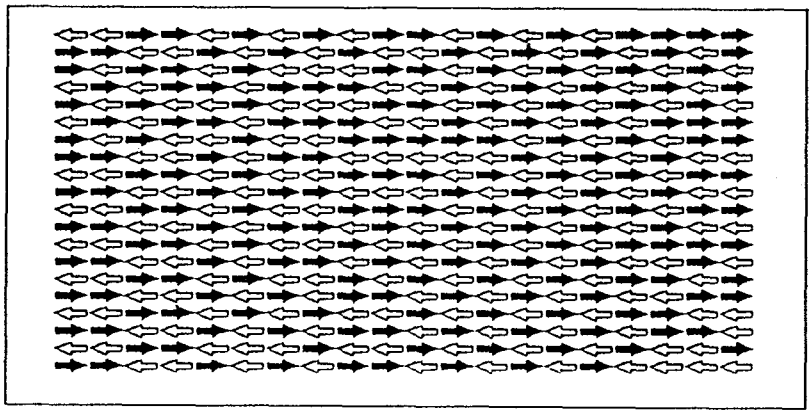

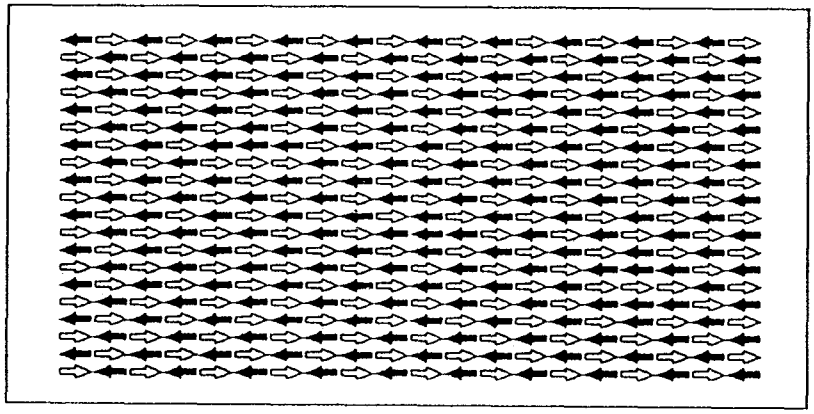

Figure 3.6: Snap shots for the parameter set(I)

The temperature is estimated with the assumption that $T_t = 200$.

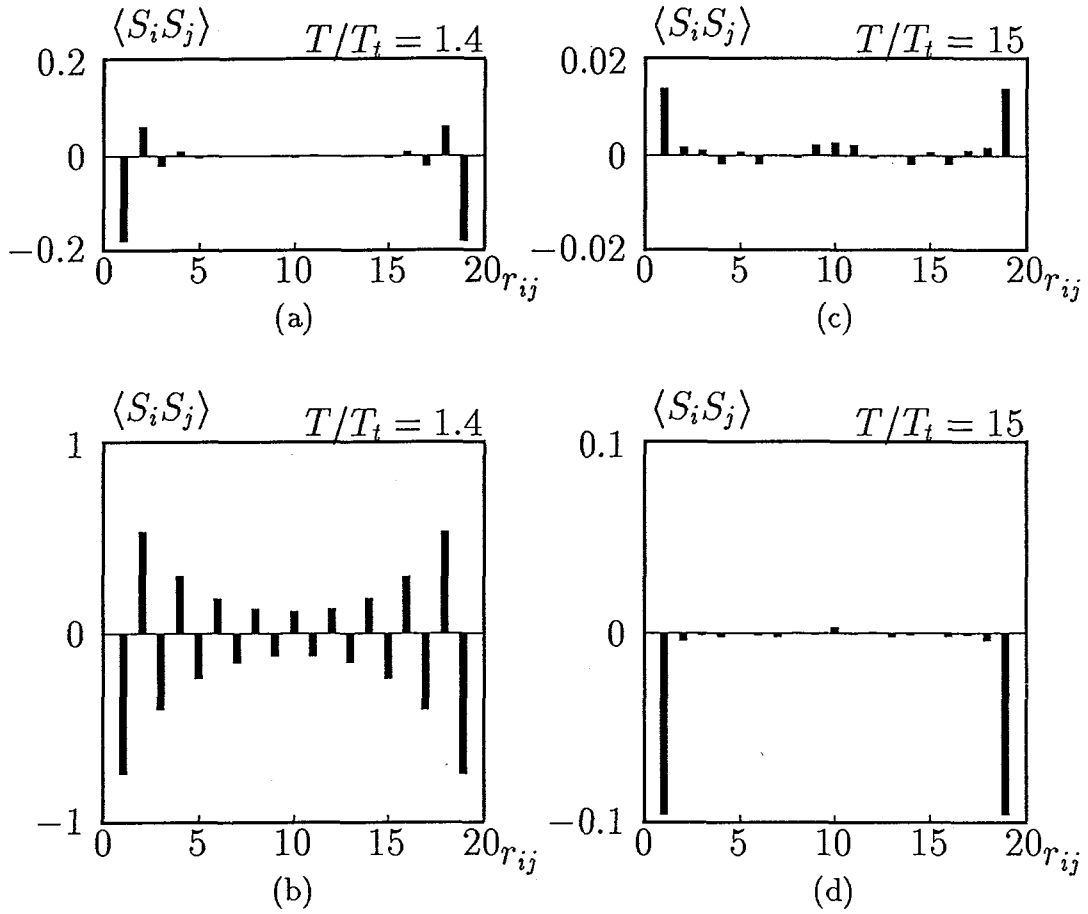

Figure 3.7: Corelation function for parameter set(I)

(a) and (b) is the correlation function between dimer rows and in a dimer row at $T/T_t = 1.4$, respectively. (c) and (d) is ones at $T/T_t = 15$. The distance is scaled by the lattice constant along each direction.

from the LEED experiment[26], that temperature, $T/T_t = 1.5$ is corresponding to about the room temperature.

It shows that the strong short rang order exists even at high temperatures, $(T/T_t > 1.0)$. The spins in the same dimer row is partially arranged an *antiferro magnetic* chain. Particularly at near the transition temperature, and such a small system as 20×20 which is used in this simulation, the correlation of spins extends all over the system and the one dimensional *antiferro magnetic* chains are formed everywhere in the system. Of course the correlation between dimer rows exists but is still very weak.

The structure factor, $F(\boldsymbol{k})$, shown in Figure 3.8, which is calculated for the parameter set (I), is defined as

$$F(\boldsymbol{k}) = \frac{1}{N}\langle|\sum_{\boldsymbol{r}_i} S_i e^{i\boldsymbol{k}\cdot\boldsymbol{r}_i}|^2\rangle, \tag{3.4}$$

$$= 1 + \sum_{\boldsymbol{r}_{ij}} \langle S_i S_j\rangle e^{i\boldsymbol{k}\cdot\boldsymbol{r}_{ij}}, \tag{3.5}$$

where $\boldsymbol{r}_{ij} = \boldsymbol{r}_i - \boldsymbol{r}_j$ and N is the number of spins. It shows a large peak along the $\bar{J}'$ to the $\bar{K}$ point in the surface Brillouin zone, which is in agreement with the streak structure observed by LEED.

The temperature dependence of the structure factor at the symmetry points, $\bar{J}$, $\bar{J}'$ and $\bar{K}$ in the surface Brillouin zone is shown in Figure 3.9.

There is the fundamental spot of 2×1 structure at the $\bar{\Gamma}$ point, so the structure factor at that point is not discussed.

The structure factor at the $\bar{K}$ point is corresponding to the staggered magnetization of the antiferromagnetic system. It is almost zero at $T \gg T_t$ because of the random arrangement of spins and increases rapidly near $T = T_t$. This shows

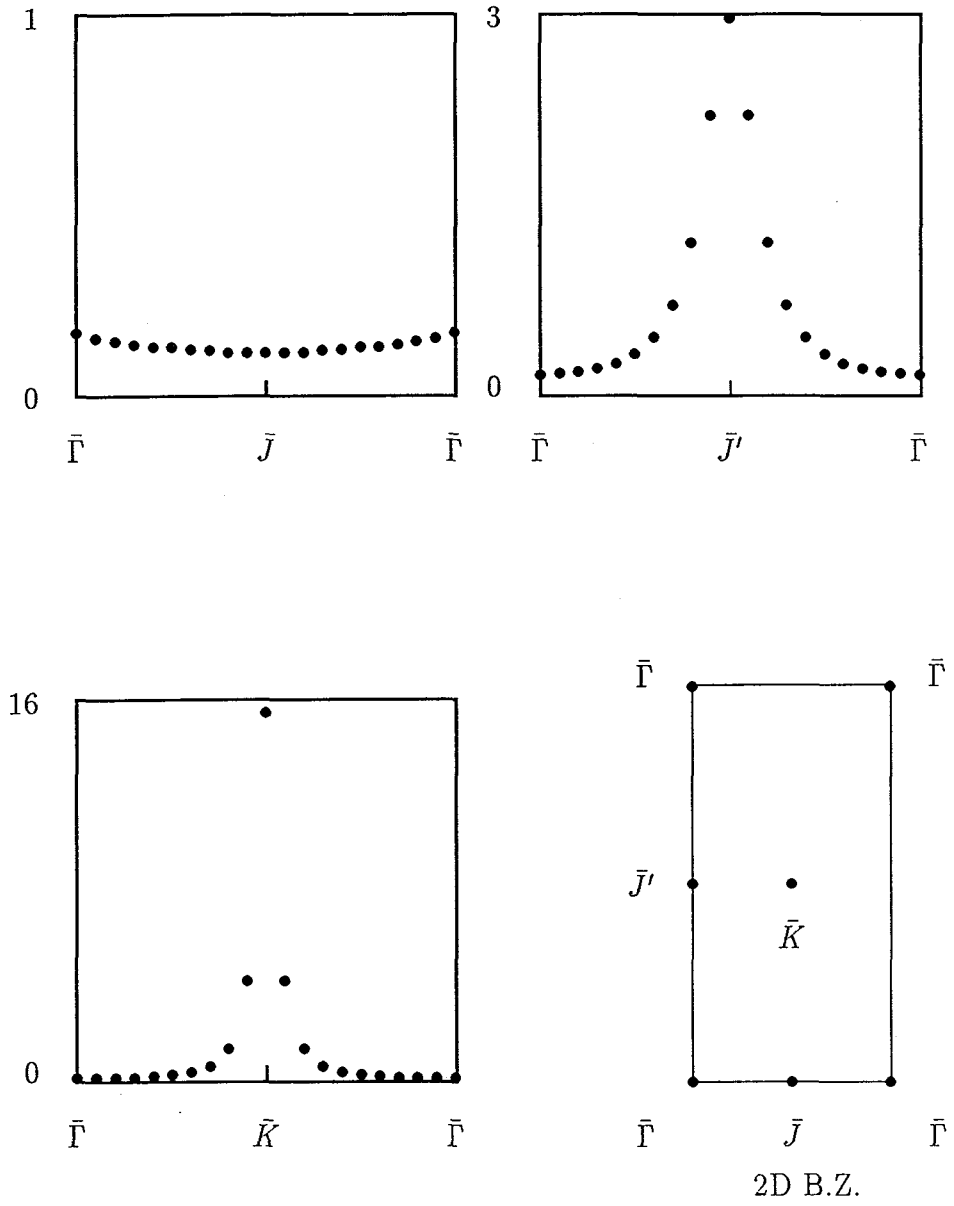

Figure 3.8: The structure factor at $T/T_t = 1.4$ for the parameter set (I)

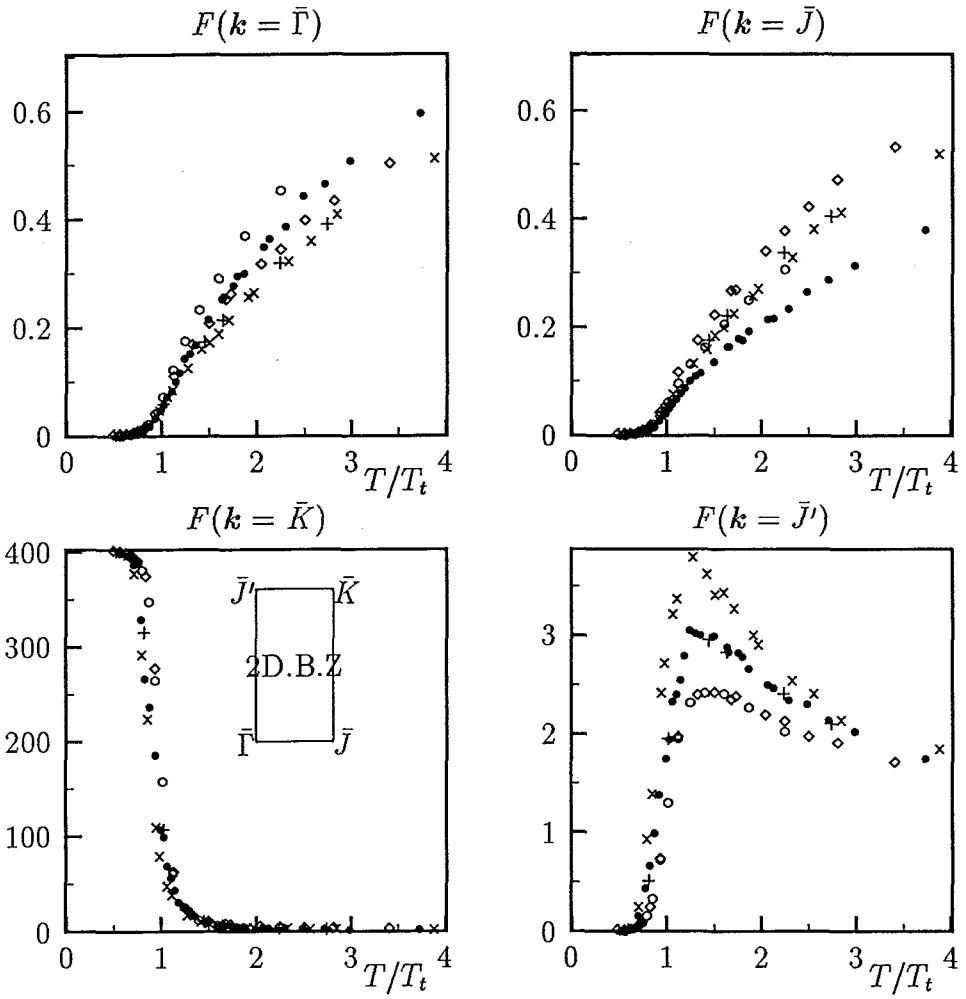

Figure 3.9: The structure factor at symmetric points

the phase transition to the c(4×2) ordered state. It becomes such a large number determined by the system size bellow $T = T_t$ that it is difficult to discuss the detail of its behavior there. The structure factor on the $\bar{J}'$ point increases slowly with the formation of the one dimensional *antiferro* chains as the temperature decreases. It has the peak at $T = T_t$ and goes to zero bellow $T = T_t$ because of the extinction rule on the c(4×2) ordered state. The structure factor on the $\bar{J}$ point gives only a back ground, which represents the degree of disorder of the system, in all temperature region. It goes to zero bellow $T = T_t$ because of the transition to the long range ordered state.

The variation of the structure factor at several temperatures is shown by the stereograph in Figure 3.10. This is in good agreement with the qualitative behavior of the streak structure in the experimental results by LEED[26].

3.2.5 Discussion

The clear difference between the system with dipole-dipole interaction and the system with only near neighbor interaction is not found qualitatively in the quantities like the energy and the specific heat as in Figure 3.5. Here, we are going to examine the effects due to the dipole-dipole interaction in the two spin correlation function. We consider only two sets of the interaction parameters as the Table 3.1(b), which is determined in such a way that

$$\frac{J^{(d)}(\bar{\Gamma}) - J^{(d)}(\bar{K})}{J^{(s)}(\bar{\Gamma}) - J^{(s)}(\bar{K})} = \frac{J^{(d)}(\bar{\Gamma}) - J^{(d)}(\bar{J}')}{J^{(s)}(\bar{\Gamma}) - J^{(s)}(\bar{J}')},$$

where $J^{(d)}(\bar{\Gamma})$ etc. are values of the Fourier components of the interaction for the two set (s) and (d) at the symmetry points in the surface Brillouin zone. The values

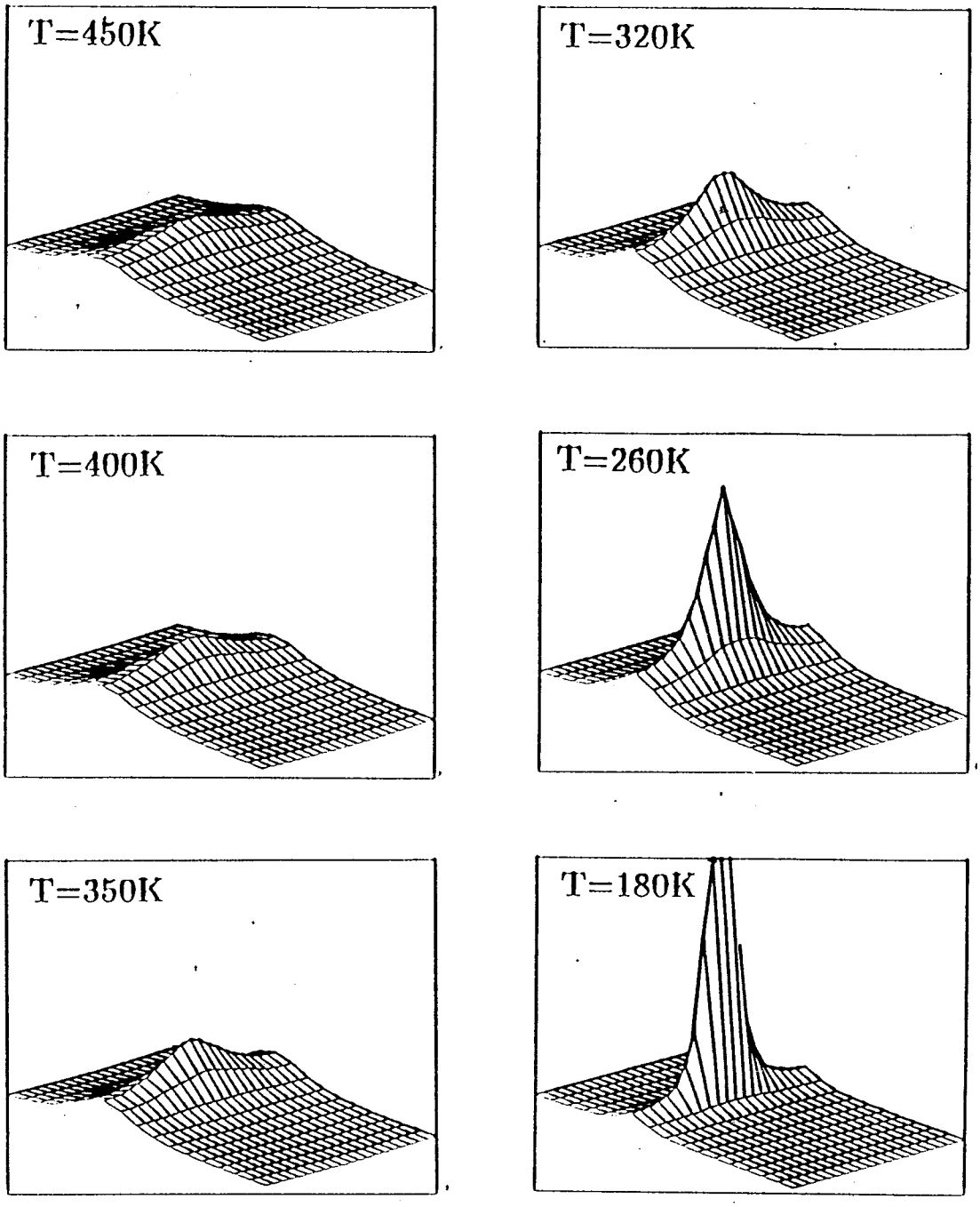

Figure 3.10: Stereograph of diffuse LEED for Si(100)

Calculations are made for the parameter set (I) in Table 3.1. The temperatures are estimated with the assumption of $T_i = 200K$. The stereograph is drawn on the unit cell of the reciprocal lattice. The long side and the short side are $\bar{\Gamma} - \bar{J}' - \bar{\Gamma}$ and $\bar{\Gamma} - \bar{J} - \bar{\Gamma}$ line, respectively.

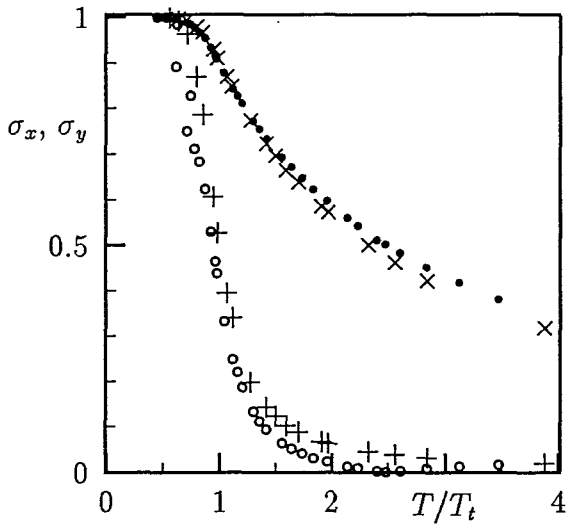

Figure 3.11: The short range order parameters

o and • are σ_x and σ_y in the (d) set and + and × are those in the (s) set.

of T_t for those two sets are obtained from the specific heat peak where $k_B = 1$.

The two spin correlation function, $\langle S_i S_j \rangle$, and the structure factor, $F(k)$, are obtained at several temperatures above T_t for the (s) and (d) sets. The short range order parameters, σ_y and σ_x, which are defined by the absolute value of the two spin correlation function for the nearest neighbor pair along the x and y-axis, respectively, are obtained as functions of temperature. The temperature dependence of σ_x and σ_y is shown in Figure 3.11. The short range order parameters are not quite different between the two parameter sets in the quantities. Although it seems that the short range order of the (d) set is more enhanced in the dimer row and prohibited between dimer rows, that difference may be within the error of this calculation.

Both of them show that there is a strong short range order in the dimer row even at high temperatures and there is almost no correlation between dimer rows until near the transition temperature. For example, we have $\sigma_x \approx 0$ and $\sigma_y \approx 0.6$ at $T/T_t = 2$ in the both sets.

The temperature dependence of the structure factor at the symmetric points in the surface Brillouin zone is shown in Figure 3.12. The delicate difference is found at the $\bar{J}$ point. But the Si(100) surface has two equivalent domains perpendicular intersecting each other and this point will be shaded by the $\bar{\Gamma}$—$\bar{J}'$ line of the opposite domain. The single domain has been obtained by an ingenious method of an electric current effect for stepped surfaces[27], but the LEED diffuse measurement has not been made yet.

3.2.6 Correlation length

When we have well developed correlation between spins, the wave vector dependence of the structure factor around the $\bar{K}$ point in the surface Brillouin zone may be described approximately by the Lorentzian as

$$F(\boldsymbol{k}) \sim \frac{C}{\varepsilon(k_x - k_x^{(M)})^2 + (k_y - k_y^{(M)})^2 + \xi^2}, \tag{3.6}$$

where k_x and k_y are x and y components of the vector $\boldsymbol{k}$. $\boldsymbol{k}^{(M)}$ is the wave vector which represents $\bar{K}$ point and $\boldsymbol{k}^{(M)} = (\frac{\pi}{2a_0}, \frac{\pi}{a_0})$. ξ^{-1} is corresponding to the correlation length along the y-axis and ε is a parameter representing the anisotropy of the two spin correlation. The correlation length along the x-axis is denoted by $\xi^{-1}\sqrt{\varepsilon}$.

This Lorentzian fitting is valid for the wave vector near the $\bar{J}'$—$\bar{K}$ line in the surface Brillouin zone as shown in Figure 3.13.

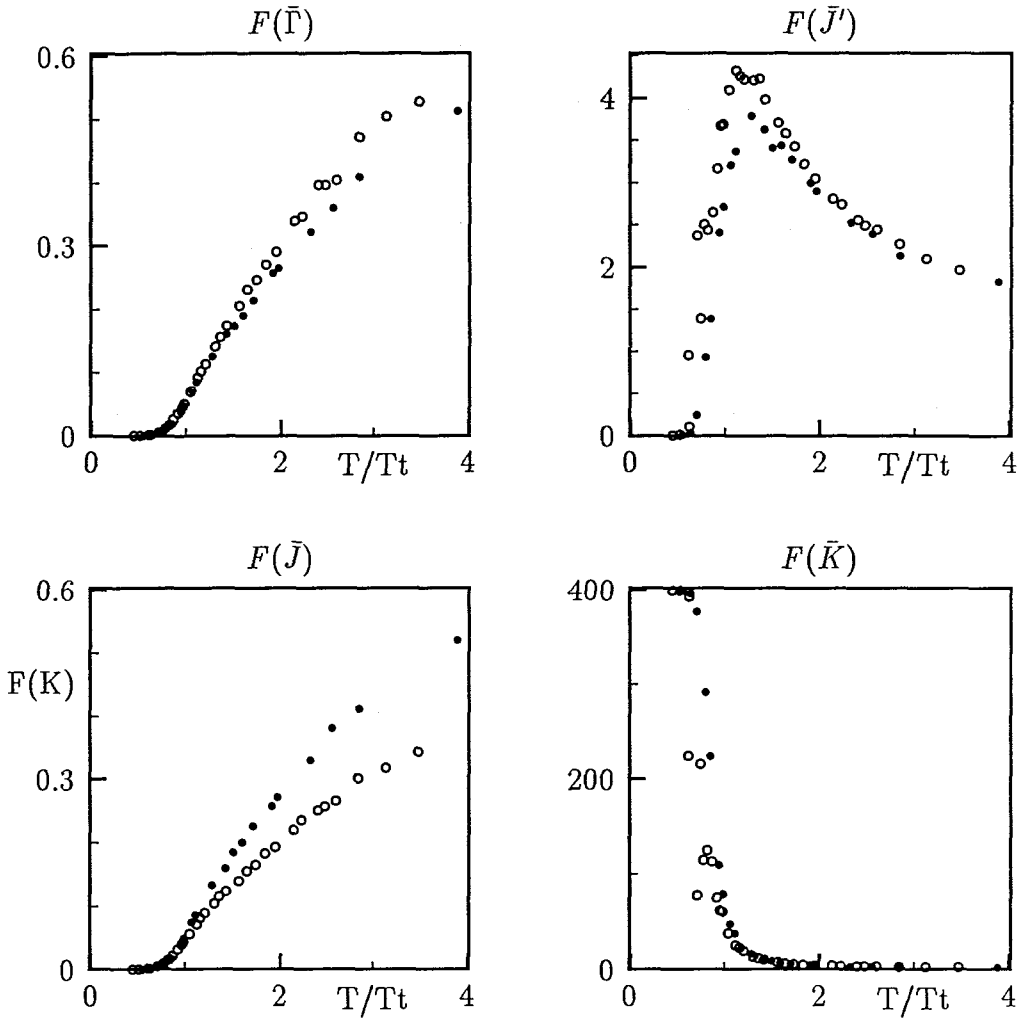

Figure 3.12: The structure factor at $\bar{J}$, $\bar{J}'$ and $\bar{K}$ (II)

o and • are the results for (d) set and (s) set,respectively.

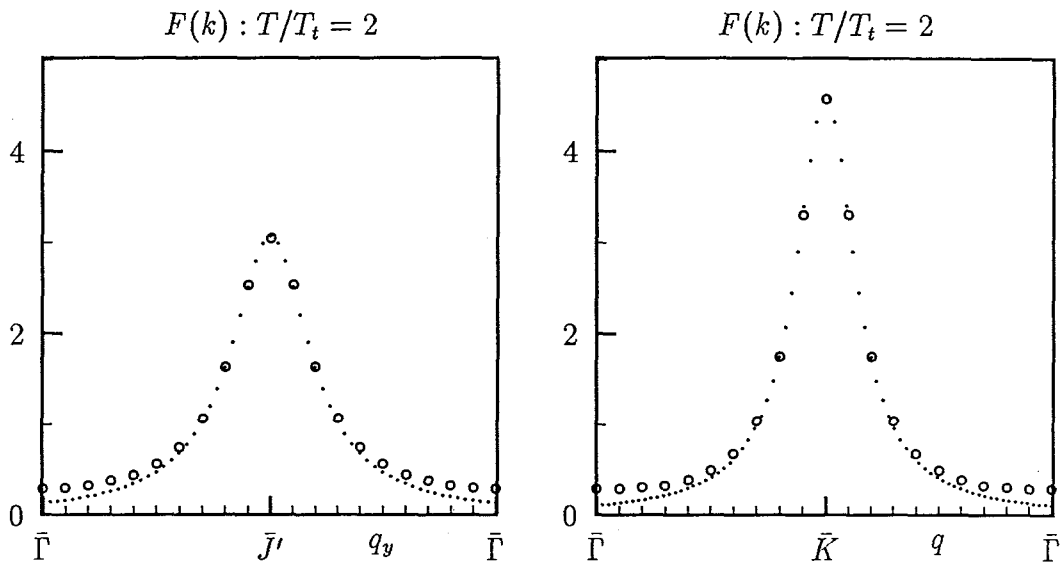

Figure 3.13: The Lorentzian fitting of the structure factor

The circle means $F(\boldsymbol{k})$ calculated by Monte Carlo simulation for the parameter (d) set at $T/T_t = 2.0$. The dot shows the Lorentzian fit by the least square means method on $\bar{\Gamma}$—$\bar{J}'$ and $\bar{\Gamma}$—$\bar{K}$ line. The fitting performed with the central five data points.

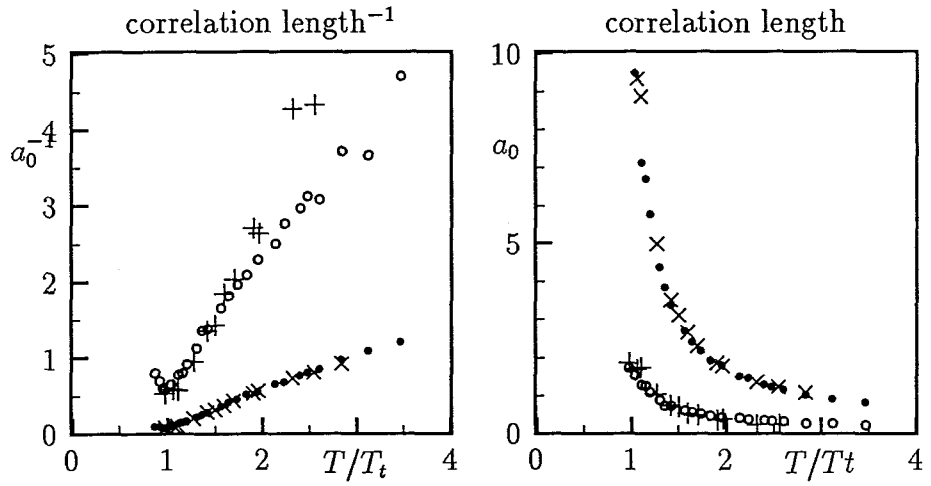

Figure 3.14: Temperature dependence of correlation length

o and • represent ξ and $\xi/\sqrt{\varepsilon}$ in the (d) set, and + and × represent ξ and $\xi/\sqrt{\varepsilon}$ in the (s) set, respectively.

The temperature dependence of the correlation length is shown in Figure 3.14. In both parameter set (s) and (d), It is found that the correlation length along the dimer row approaches the system size near the transition temperature. However the correlation length that describes the correlation between dimer rows remains the distance of the near neighbor even near the transition temperature in this simulation with the finite size system. This strong anisotropy is in good agreement with the LEED results[26]

3.3 Conclusion

The qualitative behavior of the calculated correlation function and structure factor is in good agreement with the temperature dependence of the LEED pattern. Almost

all properties of the model with dipole-dipole interaction have the same behavior as the model with only near neighbor interaction qualitatively although some difference are seen.

The larger anisotropy is needed apparently to explain quantatively the results of LEED. There are two ways to increase the anisotropy in the interactions in our limited two models. In the (s) set, we have to go to a smaller J_x values and, in the (d) set, to a smaller values in the difference between $|J_x|$ and $|J^{(d)}(\bar{J}') - J^{(d)}(\bar{M})|$. Such a small J_x value will be unlikely in the Si(100) surface. Probably the latter cancellation type might be likely in either cases where the dipole-dipole interaction is involved or not. It is remarkable that the dipole-dipole interaction with supplemented short range interactions can put such a large anisotropy into the model.

Chapter 4

Summary

The set of integral equations has been derived by use of diagramatical procedures on the bases of the high temperature expansion as well as the temperature Green function method. The two adsorbate correlation function has been obtained from the set of approximate integral equations guessed from the high temperature expansion series at low coverages of adsorbates having the repulsive dipole-dipole interaction. The results show a reasonable behavior in temperature and coverage dependence.

The errors in the solutions are estimated from the expression obtained by the Kirkwood method. These solutions are good approximation at low coverages and high temperature within Kirkwood approximation.

The repulsive dipole-dipole interaction makes the adsorbate not to come to neighbor sites even at low coverages and high temperature. The calculated structure factor shows the diffuse ring pattern because of such a strong short range order. Some calculated diffuse ring patterns are shown with the dynamic form factor. They are very sensitive to the environment of the adsorption site and the comparison of the theory and the experimental LEED pattern will give us more information about the adsorbate system.

The local structural information of the Si(100) 2×1 surface is obtained by the two spin correlation function, where the asymmetric dimer model on Si(100) is considered with the Ising spin system. The computer simulation with the Monte Carlo method is performed on the assumption that the two spin interaction is including the dipole-dipole interaction. The calculated correlation function and the structure factor are in good agreement with the LEED results. The correlation function shows that this system has a very anisotropic short range ordering. The structure factor can explain the temperature dependence of the streak pattern of LEED.

There is no remarkable effect found by the dipole-dipole interaction for the energy and the specific heat. The structure factor, however, has the delicate modification by the dipole-dipole interaction.

Appendix A

Terms of high temperature expansion

Here we list up the high temperature expansion results. The partition function of the interacting system describing in previous section is expanded up to 4th order as follows.

$$
\begin{aligned}
\frac{\Xi}{\Xi_0} &= \langle e^{-\frac{\beta}{2}\sum J_{ij}n_in_j}\rangle \\
&= 1 - 2\left(\frac{\beta}{2}\right)\sum J_{12}c^2 \\
&+ \frac{1}{2!}\left(\frac{\beta}{2}\right)^2\left[\sum J_{12}J_{34}c^4 + 4\sum J_{ij}J_{j2}c^3(1-c) + 2\sum (J_{12})^2c^2(1-c)^2\right] \\
&- \frac{1}{3!}\left(\frac{\beta}{2}\right)^3\left[\sum J_{12}J_{34}J_{56}c^6 + 12\sum J_{12}J_{34}J_{45}c^5(1-c)\right. \\
&+ 8\sum J_{12}J_{13}J_{14}c^4(1-c)(1-2c) + 24\sum J_{12}J_{23}J_{34}c^4(1-c)^2 \\
&+ 6\sum J_{12}(J_{34})^2c^4(1-c)^2 + 8\sum J_{12}J_{23}J_{31}c^3(1-c)^3 \\
&+ \left. 24\sum J_{12}(J_{23})^2c^3(1-c)^2(1-2c) + 4\sum (J_{12})^3c^2(1-c)^2(1-2c)^2\right] \\
&+ \frac{1}{4!}\left(\frac{\beta}{2}\right)^4\left[\sum J_{12}J_{34}J_{56}J_{78}c^8 + 24\sum J_{12}J_{34}J_{56}J_{67}c^7(1-c)\right. \\
&+ 96\sum J_{12}J_{34}J_{45}J_{56}c^6(1-c)^2 + 32\sum J_{12}J_{34}J_{35}J_{36}c^6(1-c)(1-2c) \\
&+ 48\sum J_{12}J_{23}J_{45}J_{56}c^6(1-c)^2 + 12\sum J_{12}J_{34}(J_{56})^2c^6(1-c)^2 \\
&+ \left. 192\sum J_{12}J_{23}J_{34}J_{35}c^5(1-c)^2(1-2c) + 32\sum J_{12}J_{34}J_{45}J_{53}c^5(1-c)^3\right.
\end{aligned}
$$

$$
\begin{aligned}
&+ \; 96\sum J_{12}(J_{34})^2 J_{45} c^5(1-c)^2(1-2c) + 48\sum J_{12}J_{23}(J_{45})^2 c^5(1-c)^3 \\
&+ \; 192\sum J_{12}J_{23}J_{34}J_{45}c^5(1-c)^3 + 16\sum J_{12}J_{13}J_{14}J_{15}c^5(1-c)(1-6c+6c^2) \\
&+ \; 96\sum (J_{12})^2 J_{23}J_{24}c^5(1-c)^2(1-6c+6c^2) + 48\sum J_{12}J_{23}J_{34}J_{41}c^4(1-c)^4 \\
&+ \; 96\sum J_{12}(J_{23})^2 J_{34}c^4(1-c)^2(1-2c)^2 + 192\sum J_{12}J_{23}J_{34}J_{42}c^4(1-c)^3(1-2c) \\
&+ \; 192\sum (J_{12})^2 J_{23}J_{34}c^4(1-c)^3(1-2c) + 12\sum (J_{12})^2 (J_{34})^2 c^4(1-c)^4 \\
&+ \; 16\sum (J_{12})^3 J_{34}c^4(1-c)^2(1-2c)^2 + 96\sum (J_{12})^2 J_{23}J_{31}c^3(1-c)^3(1-2c)^2 \\
&+ \; 48\sum (J_{12})^2 (J_{23})^2 c^3(1-c)^3(1-6c+6c^2) \\
&+ \; 96\sum (J_{12})^3 J_{23}c^3(1-c)(1-2c)(1-6c+6c^2) \\
&+ \; 8\sum (J_{12})^4 c^2(1-c)^2(1-6c+6c^2)\Big],
\end{aligned}
$$

where Ξ and Ξ_0 are the partition function of the interacting and non-interacting system respectively and c is the average particle density in the non-interacting system, defined by

$$
c = \frac{1}{e^{-\beta\mu}+1}.
$$

Then Ξ is expressed by summation of only linked clusters in the exponent as follows,

$$
\begin{aligned}
\frac{\Xi}{\Xi_0} &= \exp\left[-\beta\sum J_{ij}c^2 + \frac{1}{2!}\left(\frac{\beta}{2}\right)^2\left[4\sum J_{ij}J_{j2}c^3(1-c) + 2\sum (J_{ij})^2 c^2(1-c)^2\right]\right. \\
&- \; \frac{1}{3!}\left(\frac{\beta}{2}\right)^3\left[8\sum J_{12}J_{13}J_{14}c^4(1-c)(1-2c) + 24\sum J_{12}J_{23}J_{34}c^4(1-c)^2\right. \\
&+ \; 8\sum J_{12}J_{23}J_{31}c^3(1-c)^3 + 24\sum J_{12}(J_{23})^2 c^3(1-c)^2(1-2c) \\
&+ \; \left.4\sum (J_{12})^3 c^2(1-c)^2(1-2c)^2\right] \\
&+ \; \frac{1}{4!}\left(\frac{\beta}{2}\right)^4\left[192\sum J_{12}J_{23}J_{34}J_{35}c^5(1-c)^2(1-2c)\right. \\
&+ \; \left.192\sum J_{12}J_{23}J_{34}J_{45}c^5(1-c)^3 + 16\sum J_{12}J_{13}J_{14}J_{15}c^5(1-c)(1-6c+6c^2)\right.
\end{aligned}
$$

$$
\begin{aligned}
&+ \; 96\sum(J_{12})^2 J_{23}J_{24}c^5(1-c)^2(1-6c+6c^2) + 48\sum J_{12}J_{23}J_{34}J_{41}c^4(1-c)^4 \\
&+ \; 96\sum J_{12}(J_{23})^2 J_{34}c^4(1-c)^2(1-2c)^2 + 192\sum J_{12}J_{23}J_{34}J_{42}c^4(1-c)^3(1-2c) \\
&+ \; 192\sum(J_{12})^2 J_{23}J_{34}c^4(1-c)^3(1-2c) + 96\sum(J_{12})^2 J_{23}J_{31}c^3(1-c)^3(1-2c)^2 \\
&+ \; 48\sum(J_{12})^2(J_{23})^2 c^3(1-c)^3(1-6c+6c^2) \\
&+ \; 64\sum(J_{12})^3 J_{23}c^3(1-c)(1-2c)(1-6c+6c^2) \\
&+ \; 8\sum(J_{12})^4 c^2(1-c)^2(1-6c+6c^2)\Big]\Big].
\end{aligned}
$$

As in the partition function, the coverage θ and the correlation function can be expanded up to the 3rd order as

$$
\begin{aligned}
\theta \;&\equiv\; \langle n_i \rangle \\
&= \; c - \beta\sum J_{i1}c^2(1-c) + \frac{1}{2!}\left(\frac{\beta}{2}\right)^2\Big[8\sum J_{i1}J_{12}c^3(1-c)^2 \\
&+ \; 4\sum J_{i1}J_{i2}c^3(1-c)(1-2c) + 4\sum(J_{i1})^2 c^2(1-c)^2(1-2c)\Big] \\
&- \; \frac{1}{3!}\left(\frac{\beta}{2}\right)^3\Big[24\sum J_{i1}J_{i2}J_{12}c^3(1-c)^3(1-2c) + 48\sum J_{i1}J_{12}J_{23}c^4(1-c) \\
&+ \; 48\sum J_{i1}J_{i2}J_{23}c^4(1-c)^2(1-2c) + 24\sum J_{i1}J_{12}J_{13}c^4(1-c)^2(1-2c) \\
&+ \; 8\sum J_{i1}J_{i2}J_{i3}c^4(1-c)(1-6c+6c^2) + 24\sum(J_{i1})^2 J_{12}c^3(1-c)^2(1-2c)^2 \\
&+ \; 24\sum(J_{i1})^2 J_{i2}c^3(1-c)^2(1-6c+6c^2) + 24\sum J_{i1}(J_{12})^2 c^3(1-c)^3(1-2c) \\
&+ \; 8\sum(J_{i1})^3 c^2(1-c)^2(1-2c)(1-6c+6c^2)\Big],
\end{aligned}
$$

and

$$
\begin{aligned}
\langle n_i n_j \rangle \;&=\; c^2 - \left(\frac{\beta}{2}\right)\Big[4\sum J_{i1}c^3(1-c) + 2\sum J_{ij}c^2(1-c)^2\Big] \\
&+ \; \frac{1}{2!}\left(\frac{\beta}{2}\right)^2\Big[8\sum J_{i1}J_{i2}c^4(1-c)(1-2c) + 4\sum J_{i1}J_{2j}c^4(1-c)^2
\end{aligned}
$$

$$
\begin{aligned}
&+ \ 8\sum J_{i1}J_{1j}c^3(1-c)^3 + 16J_{ij}\sum J_{i1}c^3(1-c)^2(1-2c) \\
&+ \ 16\sum J_{i1}J_{12}c^4(1-c)^2 + 8\sum J_{i1}^2c^3(1-c)^2(1-2c) \\
&+ \ 4J_{ij}^2c^2(1-c)^2(1-2c)^2\Big] \\
&+ \ \frac{1}{3!}\left(\frac{\beta}{2}\right)^3\Big[48\sum J_{i1}^2J_{i2}c^4(1-c)^3(1-2c) + 96\sum J_{i1}J_{12}J_{23}c^5(1-c)^3 \\
&+ \ 96\sum J_{i1}J_{i2}J_{2j}c^4(1-c)^3(1-2c) + 96J_{ij}\sum J_{i1}J_{12}c^4(1-c)^3(1-2c) \\
&+ \ 48\sum J_{i1}J_{12}J_{1j}c^4(1-c)^3(1-2c) + 48\sum J_{i1}^2J_{i2}c^4(1-c)^2(1-6c+6c^2) \\
&+ \ 48\sum J_{i1}^2J_{12}c^4(1-c)^2(1-2c)^2 + 96\sum J_{i1}J_{12}J_{i3}c^5(1-c)^2(1-2c) \\
&+ \ 96\sum J_{i1}J_{12}J_{3j}c^5(1-c)^3 + 48\sum J_{i1}J_{12}J_{13}c^5(1-c)^2(1-2c) \\
&+ \ 48J_{ij}^2\sum J_{i1}c^3(1-c)^2(1-2c)(1-6c+6c^2) + 48\sum J_{i1}J_{ij}J_{2j}c^4(1-c)^2(1-2c)^2 \\
&+ \ 16\sum J_{i1}J_{i2}J_{i3}c^5(1-c)(1-6c+6c^2) + 48\sum J_{i1}J_{i2}J_{3j}c^5(1-c)(1-2c) \\
&+ \ 48\sum J_{i1}J_{12}J_{2j}c^4(1-c)^4 + 48\sum J_{i1}^2J_{1j}c^3(1-c)^3(1-2c)^2 \\
&+ \ 48J_{ij}\sum J_{i1}^2c^3(1-c)^3(1-6c+6c^2) + 48\sum J_{i1}J_{12}^2c^4(1-c)^3(1-2c) \\
&+ \ 48\sum J_{i1}J_{i2}J_{12}c^4(1-c)^3(1-2c) + 48J_{ij}\sum J_{i1}J_{1j}c^3(1-c)^3(1-2c)^2 \\
&+ \ 16\sum J_{i1}^3c^3(1-c)^2(1-2c)(1-6c+6c^2) + 8J_{ij}^3\sum c^2(1-c)^2(1-6c+6c^2)^2\Big] .
\end{aligned}
$$

Thus assuming that the coverage is small, one can be the following series for the correlation function from the result of the high temperature expansion.

$$
\begin{aligned}
\langle n_\ell n_m\rangle &= \theta^2 - 2J_{\ell m}\theta^2 + \frac{4}{N}\sum_{\mathbf{k}} J(\mathrm{k})^2e^{-i\mathbf{k}\cdot\mathbf{r}_{\ell m}}\theta^3 + 2J_{\ell m}^2\theta^2 \\
&-\frac{8}{N}\sum_{\mathbf{k}} J(\mathrm{k})^3e^{-i\mathbf{k}\cdot\mathbf{r}_{\ell m}}\theta^4 - \frac{8}{N^2}\sum_{\mathbf{k}\mathbf{k}'} J(\mathrm{k})J(\mathrm{k}')J(\mathrm{k}-\mathrm{k}')e^{-i\mathbf{k}\cdot\mathbf{r}_{\ell m}}\theta^3 \\
&-\frac{8}{N}J_{\ell m}\sum_{\mathbf{k}} J(\mathrm{k})^2e^{-i\mathbf{k}\cdot\mathbf{r}_{\ell m}}\theta^3 - \frac{4}{3}J_{\ell m}^3\theta^2 + \frac{8}{N}J_{\ell m}^2\sum_{\mathbf{k}} J(\mathrm{k})^2e^{-i\mathbf{k}\cdot\mathbf{r}_{\ell m}}\theta^3 \\
&+\frac{2}{3}J_{\ell m}^4\theta^2 + \frac{16}{N}\sum_{\mathbf{k}} J(\mathrm{k})^4e^{-i\mathbf{k}\cdot\mathbf{r}_{\ell m}}\theta^5 + \frac{16}{N}J_{\ell m}\sum_{\mathbf{k}} J(\mathrm{k})^3e^{-i\mathbf{k}\cdot\mathbf{r}_{\ell m}}\theta^4
\end{aligned}
$$

$$
\begin{aligned}
&+\frac{8}{N^2}\sum_{\mathbf{k}\mathbf{k}'} J(\mathrm{k})^2 J(\mathrm{k}')J(\mathrm{k}-\mathrm{k}')e^{-i\mathbf{k}\cdot\mathbf{r}_{\ell m}}\theta^4 \\
&+\frac{16}{3N^3}\sum_{\mathbf{k}\mathbf{k}'\mathbf{k}''} J(\mathrm{k})J(\mathrm{k}')J(\mathrm{k}'')J(\mathrm{k}+\mathrm{k}'+\mathrm{k}'')e^{-i(\mathbf{k}+\mathbf{k}'+\mathbf{k}'')\cdot\mathbf{r}_{\ell m}}\theta^3 \\
&+\frac{8}{N^2}\sum_{\mathbf{k}\mathbf{k}'} J(\mathrm{k})^2 J(\mathrm{k}')^2 e^{-i(\mathbf{k}-\mathbf{k}')\cdot\mathbf{r}_{\ell m}}\theta^3 \\
&+\frac{32}{N^2}\sum_{\mathbf{k}\mathbf{k}'} J(\mathrm{k}+\mathrm{k}')^2 J(\mathrm{k})J(\mathrm{k}')e^{-i\mathbf{k}'\cdot\mathbf{r}_{\ell m}}\theta^4 \\
&+\frac{16}{N^2}J_{\ell m}\sum_{\mathbf{k}\mathbf{k}'} J(\mathrm{k})J(\mathrm{k}')J(\mathrm{k}+\mathrm{k}')e^{-i(\mathbf{k}+\mathbf{k}')\cdot\mathbf{r}_{\ell m}}\theta^3 \\
&+\frac{4}{N^3}\sum_{\mathbf{k}\mathbf{k}'\mathbf{k}''} J(\mathrm{k})J(\mathrm{k}')J(\mathrm{k}'')J(\mathrm{k}+\mathrm{k}'+\mathrm{k}'')e^{-i(\mathbf{k}+\mathbf{k}')\cdot\mathbf{r}_{\ell m}}\theta^3 \\
&+\frac{16}{N^2}\sum_{\mathbf{k}\mathbf{k}'} J(\mathrm{k})J(\mathrm{k}')J(\mathrm{k}+\mathrm{k}')^2 e^{-i(\mathbf{k}+\mathbf{k}')\cdot\mathbf{r}_{\ell m}}\theta^4 \ldots,
\end{aligned}
$$

where $J(\mathrm{k})$ is a Fourier transform of $J_{\ell m}$ and its inverse transformation is defined by

$$
J_{\ell m} = \frac{1}{N}\sum_{\mathbf{k}} J(\mathrm{k})e^{-i\mathbf{k}\cdot\mathbf{r}_{\ell m}}.
$$

Reference

[1] Z.Zhu, N.Shima and M.Tsukada, Phys. Rev. B**40**, 11868(1989).

[2] H. Ishida and K. Terakura, Phys. Rev. **B36**, 4510 (1987).

[3] J. Kanamori, Solid State Commun. **50**, 363(1985).

[4] J. Kanamori and M. Okamoto, J. Phys. Soc. Jpn. **54**, 4636, 1985.

[5] V. L. Pokrovsky and G. V. Uimin, J. Phys. C: Solid State Phys. **11**, 3535 (1978).

[6] I. Langmür, J. Am. Chem. Soc. **54**, 2798 (1932).

[7] R. W. Gurney, Phys. Rev. **47**, 479 (1935).

[8] J. P. Muscat and D. M. Newns, J. Phys. **C7**, 2630 (1974).

[9] J. P. Muscat and D. M. Newns, Prog. Surf. Sci. **9**, 1 (1978).

[10] T.Tabata, T.Aruga and Y.Murata, Surf. Sci. Lett. **179**, L63(1987).

[11] R. L. Gerlach and T. N. Rhodin, Surface Sci. **17**, 32 (1969).

[12] J. Cousty, R. Riwan and P. Poukiassian, Surface Sci. **152/153**, 297 (1985).

[13] D. J. Chadi, Phys. Rev. Lett. **43**, 43, (1979).

[14] R. M. Tromp, R. J. Hamers and J. E. Demuth, Phys. Rev. Lett. **55**, 1303,

[15] T. Yamazaki and K. Cho, To be published in Surface science.

[16] F. j. Himpsel, P. Heimann, T. -C. Chang and D. E. Eastman, Phys. Rev. Lett. **45**, 1112, (1980).

[17] S. Å. Lindgren and L. Walldén, Solid State Commun. **28**, 283 (1978).

[18] S. Andersson and U. Jostell, Surface Sci. **46**, 625 (1974).

[19] T. Aruga, H. Tochihara and Y. Murata, Phys. Rev. **B34**, 8237 (1986).

[20] H. Kobayashi, The masters thesis.

[21] K. Kakitani, H. Kobayashi and A. Yoshimori, to be published in Surface Science.

[22] T. Kawamura, private communication.

[23] J. Frenkel, "Kinetic Theory of Liquids", Oxford at the Clarendon Press

[24] R.E.Schlier and H.E.Farnsworth, J. Chem. Phys. **30**, 917(1959).

[25] M.T.Yin and M.L.Cohen, Phys. Rev. B**24**, 2303(1981).

[26] M.Kubota and Y.Murata, Phys. Rev. B15 to be submitted.

[27] Y.Enta, S.Suzuki, S.Kono and T.Sakamoto, J. Phys. Soc. Jpn **59**, 657(1990).

[28] K.Inoue, M.Nakayama and H.Kawai, Surf. Sci. to be published.

[29] J.Ihm, D.H.Lee, J.D.Joannopoulos and J.J.Xiong, Phys. Rev. Lett. **51** 1872(1983).

[30] C. Domb and M. S. Green, "Phase Transitions and Critical Phenomena vol.3" Academic Press.